Physics – Uspekhi **49** (11) 1113 – 1129 (2006)

REVIEWS OF TOPICAL PROBLEMS PACS numbers: 05.30.Jp, **33.20.–t**, **36.40.–c**, **67.40–w**

Unusual rotations in helium and hydrogen nanoclusters and 'nanoscopic' superfluidity

B S Dumesh, L A Surin

DOI: 10.1070/PU2006v049n11ABEH006073

Contents

Abstract. **This paper reviews research on helium clusters (of up to 20 atoms) and molecular hydrogen clusters (of up to 17 molecules) weakly bound by van der Waals forces to a light chromophore molecule such as OCS, N_2O, CO_2, or CO. Such clusters form in supersonic gas jets and are studied through the spectrum of the particular chromophore used. It is found that as the cluster grows, its rotational frequency increases (the effective moment of inertia decreases) starting from a certain number of atoms (molecules) attached. Also, in CO-based clusters a nearly free rotation of the chromophore molecule was observed. Experimental studies of such clusters are reviewed, as are those of the N_2 – CO and CO – CO complexes in which both monomers nearly freely rotate. The relation of these rotations to the superfluidity of helium and hydrogen is discussed, and comparisons are made with spectroscopic experiments on chromophores and hydrogen clusters in liquid helium nanodroplets.**

1. Introduction

One of the most interesting aspects of nanophysics is the possibility (at least theoretically) of 'building bridges' between the microworld and the macroworld. But as nanoobjects get smaller, their properties depend more and more on surface interactions. The perfect way to avoid this problem is to study nanoclusters in a vacuum. It comes as no surprise that in recent years extensive research has been in progress in the field of liquid helium nanodroplets produced in the gas outflow (when cooled below the inversion temperature of the Joule – Thomson effect) from a nozzle into a vacuum (see the reviews [1, 2]). Here, the absorption spectra of doped molecules — chromophores — embedded in the nanodroplets are usually measured. Such studies have made it possible to estimate the minimum number of helium atoms needed for manifestation of superfluidity [3] and demonstrated a number of other striking effects. Some of these studies will be discussed below. Although the nanodroplets of interest are rather small, they nevertheless are macroobjects because the real number of their constituent atoms is no less than several hundred.

In connection with a significant progress in the techniques of gas cooling in supersonic jets over the last few years, it has become possible to produce much smaller nanoclusters of helium and molecular hydrogen (consisting of about a few to several dozen He atoms or H_2 molecules). A gas with an initial temperature of about 100 K can be cooled to several tenths of a kelvin, and clusters consisting of helium atoms attached to a chromophore molecule via the weak van der Waals force can form. The study of such clusters has only begun, [1] but already nontrivial dissipationless rotations with partial entrainment of the cluster atoms have been discovered, and the very notion of superfluidity as applied to such systems needs to be redefined. The present review describes current experiments with such nanoclusters. We also discuss the results obtained.

B S Dumesh, L A Surin Institute of Spectroscopy, Russian Academy of Sciences
142190 Troitsk, Moscow region, Russian Federation
Tel. (7-495) 334 02 39
Fax (7-495) 334 08 86
E-mail: dumesh@isan.troitsk.ru

Received 2 March 2006, revised 18 April 2006
Uspekhi Fizicheskikh Nauk **176** (11) 1137 – 1154 (2006)
Translated by E Yankovsky; edited by A Radzig

[1] The first paper [4] appeared in 2002.

It should be noted that when the coupling between helium atoms and a chromophore molecule is weak, nontrivial rotations are observed already in binary systems. For instance, nearly free rotations of the CO molecule reveal themselves in He – CO [5] and H_2 – CO [6], in addition to the complex rotating as a whole. Hence, we begin our review by examining such rotations in complexes formed by an atom and a molecule, a case that constitutes a good basis for further discussions. Such an extended introduction is useful also because experiments on the spectroscopy of weakly bound complexes have been done at the same experimental facilities and involved the same research groups as in experiments with more complex clusters consisting of dozens of helium atoms or hydrogen molecules.

2. Methods of production and aspects of spectral studies on ultracold gas jets

The binding energy of helium atoms in clusters amounts to several kelvins, so that for the clusters to form the gas should be cooled to the appropriate temperature. At present, the techniques of expanding gas with supersonic speed into a vacuum have been developed to such perfection that the desired cooling can be achieved at a moderate cost. This process is covered rather thoroughly in the literature (e.g., see Ref. [7]), so that here we will discuss it only briefly. A mixture of gaseous helium with a small chromophore impurity outflows from a supersonic nozzle with a characteristic area of 0.1 – 0.01 mm^2 into a vacuum chamber, where it adiabatically expands. If pumping the chamber rather intensively, so that the residual pressure in the chamber is on the order of 0.001 Torr, the cooling efficiency is determined mainly by the initial pressure and temperature. At an initial pressure of 50 atm and room temperature of the nozzle, the final helium temperature may be as low as 0.3 K, and if vapors of liquid nitrogen is used for cooling the nozzle the helium temperature may be as low as 0.1 K [8]. In such conditions, clusters consisting of a chromophore molecule and attached helium atoms begin to form in the jet.

The gas temperature in the jet can be estimated by measuring the difference in the populations of the rotational levels of these clusters, which determines the intensities of spectral lines. Figure 1 shows recordings of the R(0) lines (from the lowest $J = 0$ level) and Q(1) (from the $J = 1$ level with an energy of 0.8 K) in He_2 – CO [9]. The rotational temperature determined from the ratio of their intensities (on the order of 10 above noise) amounts to about 0.3 K. The lines were recorded at 50 atm as the initial pressure and at room temperature of the nozzle.

To combine the necessary gas fluxes in the jet with a reasonable pumping speed, the short-pulse regime is used. An electromagnetic valve is placed just before the nozzle's entrance and it opens the entrance to the gas for about 1 ms. An oil booster pump with an efficiency of 1000 l s^{-1} provides the necessary vacuum in the chamber with a pulse repetition rate of 1 Hz. The specific characteristics refer to the spectrometer operating in the millimeter wave range (the Köln – Troitsk Collaboration).

Spectral studies of helium clusters and binary systems have been done in the IR (A R W McKellar's group, Ottawa, Canada), the centimeter wave (W Jäger's group, Edmonton, Canada), and the millimeter wave (the Russian – German G Winnewisser – B Dumesh group, Köln – Troitsk) ranges. Since the spectral linewidths in a supersonic jet are close to the Doppler limit, all measurements are done with high-resolution spectrometers furnished with a coherent source of radiation.

A more complicated problem is how to achieve in such experiments the sensitivity needed to register the weak lines. To reach the required temperatures, the chromophore content in helium should be about 0.1%, and the concentration of the clusters that form amounts to less than 0.1% of the chromophore amount. The sensitivity of conventional single-pass spectrometers is too low for detecting such weak signals, which means devices with multiple passage of radiation through the supersonic jet should be employed. In the IR range, a spectrometer built around diode lasers with a toroidal mirror system that ensured more than 100 passes of the laser beam through the jet was used [10]. In the millimeter and centimeter wave ranges, due to the large radiation wavelength, such multipass schemes are unrealistic and the only way to reach the necessary sensitivity is to direct the jet through a high-Q open cavity filled with radiation. Highly sensitive pulsed Fourier-transform spectrometers operating in the centimeter wave range, which match very well with open cavities, have been developed by Balle and Flygare [11]. The device employed by Jäger's group belongs in particular to this type [12].

Unfortunately, these spectrometers are ineffective in the millimeter wave range, since there are no fairly powerful

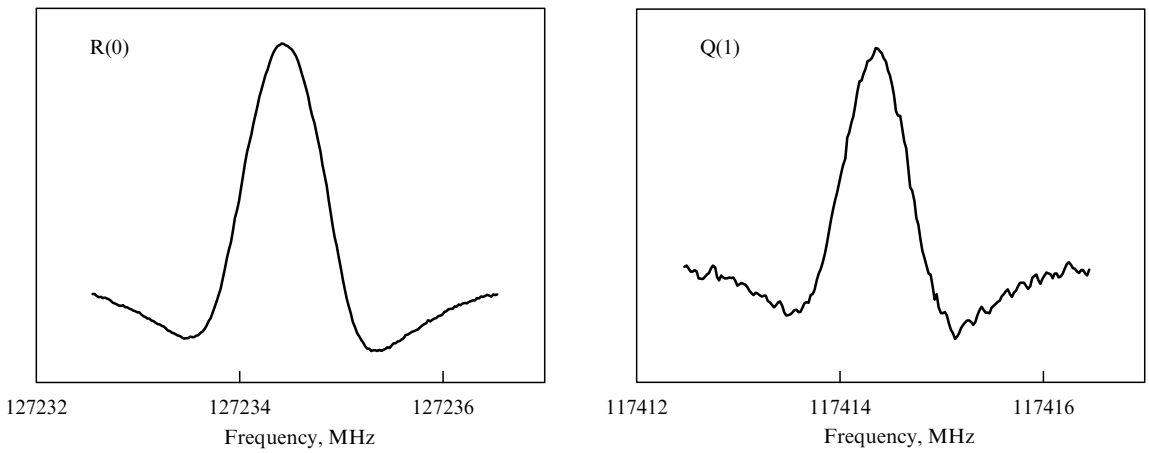

Figure 1. The rotational lines R(0) and Q(1) of the $K = 1 - 0$ band in He_2 – CO [9].

sources of radiation with sufficiently large frequency tuning. Our group has developed an intracavity spectrometer [13] based on the Soviet broadband millimeter-wave oscillator known as the orotron [14]. The device contains an own open cavity that sets the frequency of the radiation, through which the gas being studied can be directed. As a result, there are approximately one hundred effective passes of the radiation through the jet, which guarantees sufficient sensitivity of the spectrometer. Moreover, the orotron has a very narrow radiation spectrum, which allows it to achieve not only Doppler but even sub-Doppler spectral resolution [15]. The minimal absorption coefficient that was recorded with a single scan of a spectral line was $\gamma_{\min} \approx 3 \times 10^{-10}$ cm^{-1}, and the spectral resolution was 10 kHz. A description of a version of the device with a supersonic jet can be found in Ref. [16].

The double resonance method helps a lot in identifying complex spectra [17]. If one transition in a system of three levels coupled by two transitions is saturated, the level populations change, and it changes the intensity of absorption on the second transition. Hence, by tuning the spectrometer to the second transition, we can record the absorption of radiation from an additional source in the first transition by the modulation of the spectrometer's signal. In addition to being able to select the pairs of transitions belonging to a three-level system, the double resonance method makes it possible to effectively widen the spectral range under investigation and to detect transitions from the levels whose thermal populations are too low to observe them directly. The description of a device used to record double resonances and built around a pulsed Fourier-transform spectrometer can be found in Ref. [18], and that as applied to an orotron spectrometer in Ref. [19].

The problems associated with interpreting spectra and identifying molecular rotational transitions will be discussed as we go along. Notice that the close cooperation of the research groups, which included frequent consultations and the exchange of experimental data even before their publication, had a positive effect on our work.

3. Nearly free rotations of monomers in binary molecular complexes

In an overwhelming number of cases, no qualitative changes in the nature of the spectra are observed in passing from molecules to their complexes. The relative motion of the monomers usually lead only to relatively low-frequency stretching and bending vibrations [2] and, in some cases, to the tunnel type splittings if the complex consists of two identical molecules. [3] At the same time, rotational spectra of complexes correspond fairly well to models of a quasirigid rotor, i.e., they rotate as a single entity. This is natural since the van der Waals interaction of the molecules is anisotropic and orients the monomers in relation to each other fairly rigidly. The main difference between the rotation of complexes and that of molecules is the increase in centrifugal perturbation in the former case.

In recent years, however, as a result of studies of weakly bound systems of light atoms and molecules, objects have been discovered in which, in addition to the rotation of a complex as a whole, the nearly free rotation of the monomers is also detected. This is observed most evidently in the spectra of X – CO complexes, where X = H_2, D_2, He, N_2, and CO.

What makes these studies so interesting is that, first, they broaden our outlook on the possible types of molecular motion. Second, they provide a reliable basis for research into helium and hydrogen nanoclusters with embedded light chromophore molecules, research aimed at a search for hydrogen superfluidity and the study of the transient region between molecular motion and inner excitations in condensed media. Third, these complexes are of interest on their own accord because they are present (and, possibly, will be discovered) in interstellar medium, since CO is the most abundant polar molecule in interstellar space. Furthermore, N_2 – CO complexes may play a noticeable role in the optical properties of the upper atmosphere.

3.1 Rigid rotor and free rotation models

Before we begin examining the spectra of nearly free rotations of monomers, some terminology should be clarified. In molecular spectroscopy, the term 'internal rotation' has been used for a long time. Such a rotation refers to specific motion in a number of molecules whose symmetry group includes a high-order axis of symmetry. In rotations with respect to this axis, the potential energy can be interpreted as a series of potential wells in which the molecule (or its fragments) perform torsional vibrations. If the potential barriers separating the wells are not very high, tunneling between the wells is possible. Just this interesting phenomenon is known as 'internal rotation', although it generally begins to resemble rotations only at high excitation levels (e.g., see Ref. [20]).

The rotations of monomers in complexes, which are of interest to us, are commonly known as 'hindered' or 'nearly free'. The difference between these terms will soon become apparent.

We begin with a brief description of the structure of the rotational energy levels of a complex in two limiting cases: a rigid rotor, and the free rotations of a monomer. To calculate these energy levels, we should first determine the components of the inertia tensor. The shape of the X – CO complexes (X is the atom of an inert gas) is close to that of a *T*-shaped

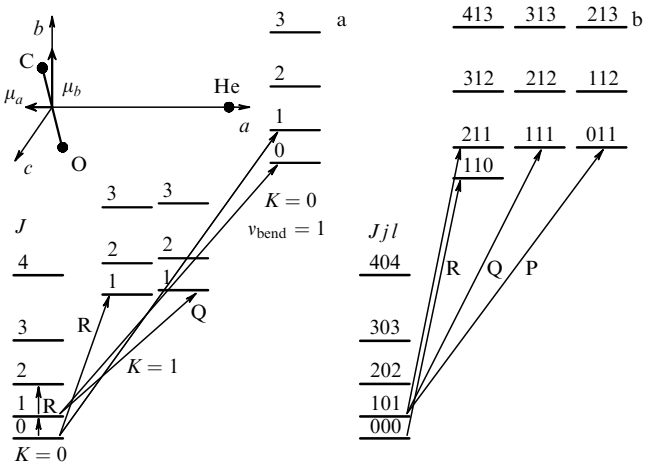

Figure 2. Diagrams of the rotational levels of a prolate, slightly asymmetric top molecule (a), and of an Rg – CO type complex with free monomer rotations (b). The arrows denote the allowed spectral transitions from the two lower energy levels. The inset shows the geometry of the He – CO complex.

[2] In stretching vibrations of a complex, it is the distance between monomers that oscillates, while the mutual orientation of monomers oscillates in bending vibrations.

[3] Such complexes are usually called dimers.

molecule (see the inset to Fig. 2), where the distance between the monomers, $R \approx 0.4$ nm, is much larger than their size r ($r_{CO} \approx 0.11$ nm). Hence, it is easy to see that the principal axes a, b, and c (in order of increasing values of the components I_a, I_b, and I_c) of the inertia tensor are arranged as follows: the a-axis passes through the attached atom, the b-axis lies in the complex's plane and is perpendicular to a, and the c-axis is perpendicular to this plane. Here, $I_a \ll I_b \approx I_c$, i.e., the inertia tensor corresponds to a heavily prolate, slightly asymmetric top, and the rotational constants (the reciprocal tensor components) are as follows: $A \approx b_{CO}$ (the rotational constant of CO), and

$$C \approx B \approx \frac{\hbar^2}{2\mu R^2}\,, \tag{1}$$

where μ is the reduced mass of the complex.

The rotational energy levels of prolate, slightly asymmetric rigid rotor can be described by the following formula [21]

$$E(J,K) = \left(A - \frac{B+C}{2}\right) K^2 + \frac{B+C}{2}\, J(J+1) \pm \left(A - \frac{B+C}{2}\right) \frac{\alpha^K}{2}\, \frac{(J+K)!}{8^K\left[(K-1)!\right]^2 (J-K)!}\,, \tag{2}$$

where J is the total angular momentum, K is its projection on the complex's axis, and $\alpha = (C-B)/(2A-B-C)$ is the asymmetry parameter. The first two terms on the right-hand side define the energy of a symmetric top molecule, and the third term gives the splitting of the doubly degenerate (at $K \neq 0$) levels due to asymmetry. In the case that is most important to us ($K = 1$) this expression becomes

$$E(J,K) = \left(A - \frac{B+C}{2}\right) + \frac{B+C}{2}\, J(J+1) \pm \frac{B-C}{4}\, J(J+1)\,. \tag{3}$$

When $A \gg B$, C, the collection of rotational levels described by these formulas conveniently splits into groups with running J and other quantum numbers being equal. We call such groups 'stacks'. A stack is characterized by its quantum number K and parity. A stack is of even parity if as a result of a rotation through π with respect to the c-axis the rotational wave functions transform as $\Psi(\pi) = (-1)^J \Psi(0)$, and of odd parity if they transform as $\Psi(\pi) = -(-1)^J \Psi(0)$. Clearly, the two split stacks at $K \neq 0$ are of different parity, and they are denoted as K_e (even) and K_f (odd). The stack with $K = 0$ is of even parity (0_e). A diagram of the rotational levels of an prolate, slightly asymmetric top is presented in Fig. 2a. For the sake of generality, we have added to them the lower rotational levels of the bending vibration.

The allowed spectral transitions are determined by the selection rules for the dipole moment μ. In the general case, one finds $\Delta J = 0, \pm 1$. Here, for e $\leftrightarrow$ e and f $\leftrightarrow$ f transitions, one has $\Delta J = \pm 1$ (the R- and P-branches), and for e $\leftrightarrow$ f transitions, $\Delta J = 0$ (Q-branches). Transitions within stacks fall basically in the centimeter wave range, while transitions between stacks fall in the millimeter and submillimeter wave ranges.

If only one monomer rotates freely, the diagram of rotational levels can easily be constructed [22, 23]. In this case there are two independent rotations: that of the monomer with the angular momentum j, and that of the entire complex with the angular momentum l (*end-over-end* rotation). Here, the energy is independent of the total angular momentum $J = j + l$:

$$E = bj(j+1) + Bl(l+1)\,, \tag{4}$$

where b is the monomer's rotational constant (in our case b_{CO}), and B is the rotational constant of the complex under the assumption (1) that the monomers are point-like objects. The selection rules in the case of free monomer rotation are formulated as

$$\Delta J = 0, \pm 1\,, \quad \Delta j = \pm 1\,, \quad \Delta l = 0\,. \tag{5}$$

To simplify matters, we examine only the case where $b \gg B$, $j = 0, 1$, which reflects fairly well all the features of such rotation and is convenient if we want to compare the results with the rigid-rotor case. In accordance with the law of addition of angular momenta, there are four sets of levels: $(J, j, l) = (J, 0, J)$; $(J, 1, J-1)$; $(J, 1, J)$, and $(J, 1, J+1)$. We can easily establish the relation to the rigid-rotor levels: $(J, 0, J)$ corresponds to (0_e), $(J, 1, J-1)$ to (1_e), and $(J, 1, J)$ to (1_f). What remains is the set $(J, 1, J+1)$ with the lower level (0, 1, 1), i.e., with the projection of the angular momentum $K = 0$. We will shortly see that as we move to the rigid-rotor case, this set transforms into the lower rotational stack ($K = 0$) of the bending vibration of the complex. Levels with equal j and l but different total angular momenta J are degenerate. Their diagram is shown in Fig. 2b. Any perturbation removes this degeneracy, but the main features of the arrangement of the energy levels for nearly free rotation of a monomer can be formulated as follows:

(1) the energy of the bending rotation nearly coincides with the energy of the 1_f state;

(2) states with $K = 1$ are above the ground state by $2b_{CO}$, i.e., lie twice as high as in the rigid-rotor case, and

(3) the splitting of the lower $K = 1$ levels is large: $E(1, 1_f) - E(1, 1_e) = 2B$.

When the anisotropy of the interaction potential between the molecule and the atom is 'switched on', the free rotation of the monomer becomes hindered and explicit dependence of the energy on J emerges. The passage to the rigid-rotor case was examined in Refs [22, 23] by looking to the perturbation theory. The researchers assumed that near the energy minimum the angular dependence of the potential, $V(\theta)$, can be expressed in the form of an expansion in terms of even powers of Legendre polynomials:

$$V(\theta) = V_2 P_2(\cos\theta) = \frac{V_2(3\cos^2\theta - 1)}{2}\,.$$

Accordingly, the Hamiltonian of the system can be written down as follows:

$$\hat{H} = b\hat{j}^2 + B\hat{l}^2 + V_2 P_2(\cos\theta)\,, \tag{6}$$

and the shifts of the energy levels caused by a perturbation are calculated on the basis of the wave functions $\Psi(J, M, j, l)$ of the complex with free monomer rotations.

The results of calculations with $b_{CO} = 1.92$ cm^{-1} and $B = 0.07$ cm^{-1} (corresponding to Ar – CO) are shown in Fig. 3 [23]. Clearly, when the interaction is switched on, the levels with $j = 1$ split, and the energy of a third of them grows, while that of the remaining two-thirds decreases, and the levels with equal values of J merge together. [4] Here this group

[4] In this model, there is no K-splitting of levels for a rigid rotor.

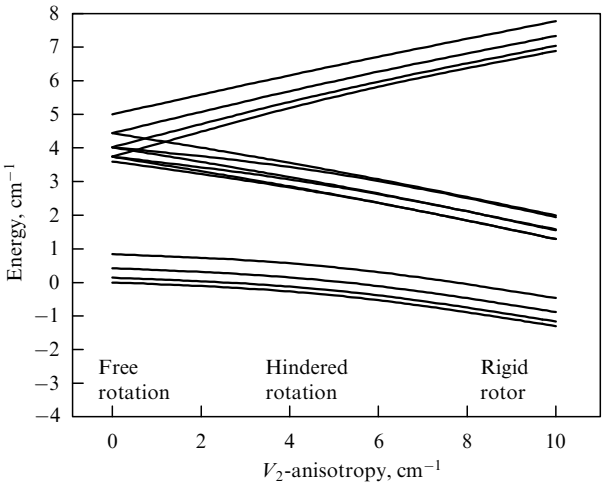

Figure 3. Transformation of the rotational levels of the Rg–CO type complexes with $j = 0$ and 1 as interaction anisotropy is 'switched on' [23].

of levels begins from $J = 1$, i.e., it indeed goes over to the states with $K = 1$. Accordingly, the states that begin from $J = 0$ and have rising energy transform into the bending vibration of the complex.

It is interesting to note that the different manifestations of free rotation disappear nonuniformly as anisotropy grows. For instance, the ratio of the bending vibration energy to the rotational energy in state 1_f becomes equal to about 2 already at $V = 4.5$ cm^{-1}, which is only slightly larger than $2b_{CO}$. At approximately the same level of anisotropy, the strong splitting of levels $(J, 1, J)-(J, 1, J-1)$ $\{1_f - 1_e\}$ also disappears. At the same time, the energy of states with $K = 1$ remains to be on the order of $1.5b_{CO}$ even at $V = 10$ cm^{-1}. It comes as no surprise that most experimental indications of hindered rotations are concerned with the anomalously high energy (compared to the value predicted for the rigid rotor) of the transitions $K = 1-0$ [23, 24].

3.2 Complexes involving one rotating monomer (He–CO and *para*H_2O–CO)

We are coming now to the comparison of the above results with available experimental data. Table 1 collates the main

Table 1. Some characteristics of Rg–CO complexes.

	Xe–CO	Kr–CO	Ar–CO	Ne–CO	^{4}He–CO	^{3}He–CO
R, Å	4.194	3.977	3.85	3.646	4.08	4.08
E_{1_e} (E_{110})	2.255	2.29	2.416	3.216	3.9965	3.9636
E_b (E_{011})	13.794	13.156	11.918	8.490	5.391	5.18
E_b/E_{1_f}	6.117	5.745	4.933	2.640	1.263	1.18
$(E_{1_f} - E_{1_e})/B$	0.034	0.042	0.062	0.134	0.94	1.17
IR	[25, 26]	[26, 29]	see Note	[31, 32]	[5, 22, 40]	[22]
MW	[27, 28]	[27, 28]	[30]	[33–36]	[40, 41]	[41]
T				[37–39]	[22, 42]	

Note. Many papers have been written concerning Ar–CO. Reviews can be found in Refs [23, 57] (see also Ref. [30]).

[5] The last three rows in Table 1 contain the references to spectroscopic data from IR and microwave (centimeter and millimeter wave ranges) measurements; T refers to the theoretical data. Since there are many theoretical works on this subject, we have listed only the latest.

Table 2. Some characteristics of *ortho*$^{14}N_2$–CO, *para*H_2–CO, and *ortho*D_2–CO complexes.

	ortho$^{14}N_2$–CO	*para*H_2–CO	*ortho*D_2–CO
R, Å	4.025	4.13	4.13
E_{1_e} (E_{110})	3.529	3.6179	3.4289
E_b (E_{011})	4.666	7.079	6.978
E_b/E_{1_f}	1.268	1.731	1.942
$(E_{1_f} - E_{1_e})/B$	0.094	0.895	0.541
IR	[43, 44, 45*]	[6, 51]	[52]
MW	[46*, 47*, 48, 49]	[53]	[54]
T	[50]	[55, 56]	

* Also including *para*N_2–CO measurements.

characteristics of the rotational spectra of CO complexes that incorporate rare gas atoms.[5] Clearly, there is a distinct correlation between a decrease in the mass of the rare gas atom and an increase in the flexibility of the complex, which is expressed in the smooth reduction in the bending-vibration frequency E_b/h and the increase in the energy of the lower $K = 1_e$ level (E_{1_e}). The record-breaker here is the He–CO complex for which $E_{1_e} > 2b_{CO}$ and $E_b/E_{1_f} = 1.26$. At the same time, for all complexes the splitting of the $K = 1$ stacks remains small ($\ll B$), with the exception of He–CO. This is rather natural since the ratio E_b/E_{1_f} and, hence, the potential's angular anisotropy are fairly large for such complexes.

Table 2 lists the data on CO complexes with the diatomic *para*H_2, *ortho*D_2, and *ortho*$^{14}N_2$ molecules. The fact that *para*- and *ortho*-modifications of the X_2 type molecules are preserved in the formation of complexes is nontrivial from the viewpoint of internal rotations since, due to permutation symmetry requirements, these molecules possess certain intrinsic angular momenta (even for *para*-states of fermions and *ortho*-bosons, and odd for *ortho*-fermions and *para*-bosons). At temperatures used in our research, only the lower rotational levels are occupied in hydrogen and nitrogen molecules, with the result that *para*H_2, *ortho*D_2, and *ortho*$^{14}N_2$ possess an intrinsic angular momentum $j = 0$, and the energy levels of CO complexes with them have the same structure as the levels in the above case of monatomic gases. Complexes with hydrogen and deuterium molecules fit nicely between helium and neon and demonstrate fairly large K-splitting. Comparison of the spectra of various isotopomers also shows that the rotational degree of freedom depends not only on the binding energy but also on the mass of the attached atom (molecule). For instance, in the *ortho*D_2–CO complex, the splitting of the lower $K = 1$ levels is twice as small as in *para*H_2–CO.

The lowest bending-vibration frequency 4.666 cm^{-1} has been detected in the *ortho*N_2–CO complex. At the same time, the K-splitting is small here and is described fairly well by formula (3), which is the standard formula for the rigid rotor, with a relatively small value of the asymmetry parameter. Also, the arrangement of the *ortho*N_2–CO levels inside stacks up to $J = 18$ [58] is described satisfactorily by power series (standard for the rigid rotor):

$$E_i(J) = \sigma_i + B_i J(J+1) - D_i J^2 (J+1)^2 + \dots . \qquad (7)$$

However, the σ_i values correspond to the case of a nearly free rotation of CO. Unfortunately, the rotational energy levels of *ortho*N_2–CO have never been calculated, and this anomalous behavior has yet to find an explanation.

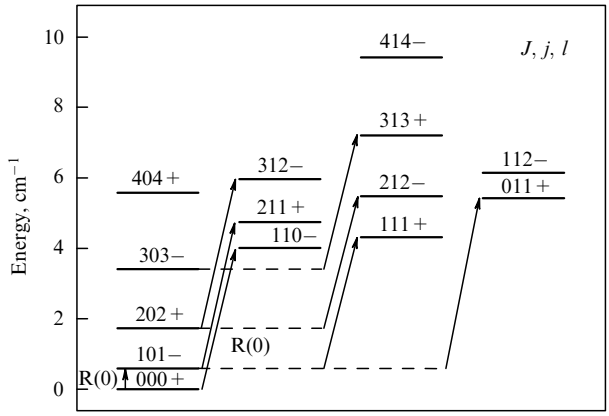

Figure 4. Diagram of the ^{4}He – CO rotational levels [5]. The arrows denote the measured rotational transitions [40, 41].

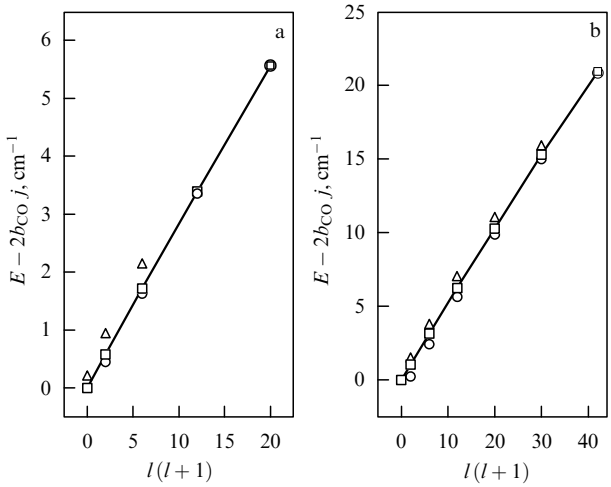

Figure 5. Dependence of the energy of the rotational levels of ^{4}He – CO (a) and *para*H$_2$ – CO (b) on the quantum number l (rotation of the complex as a whole): □ — $(J, 0, J)$, ○ — $(J, 1, J)$, and △ — $(J, 1, J-1)$.

The spectra of the ^{4}He – ^{12}C^{16} and ^{3}He – ^{12}C^{16}O complexes have been measured in the IR range by Chan and McKellar [5] and Chuaqui et al. [22], and in the millimeter wave range by Surin et al. [41]. McKellar et al. [40] measured the IR spectra of the ^{4}He – ^{13}C^{16}O complexes and the transition (101) ← (000) (the centimeter wave range) for ^{4}He complexes with different isotopic modifications of the CO molecule. Figure 4 illustrates the diagram of the ^{4}He – CO rotational levels obtained from data on IR spectra [5] and indicates the measured rotational transitions [40, 41]. What is interesting is that all the energy levels of this complex are shown, since at higher excitations the complex breaks down. At first glance this pattern resembles the arrangement of the rotational energy levels of a heavily prolate, slightly asymmetric top. At the bottom are the $K = 0$ levels, a little higher there are the 1_e and 1_f states (which are close in energy), and even higher (but not so high as could be expected) is the bending vibration in the $K = 0$ rotational state.

However, the energy of the lower $K = 1$ level (1, 1, 0) is even higher than the energy of free CO rotations ($2b_{CO}$). This feature can be explained by the shift in the energy of the lowest level (0, 0, 0), which always decreases in a perturbation-theory treatment. What is interesting, however, is that when more He atoms are added to CO, the increase in the energy of the level (1,1,0) continues [59].

What also strikes the eye is that the dependence of the energy on J differs markedly from stack to stack. This is quite natural for the nearly-free-rotation model, since the rotational energy basically depends on l rather than on J [see formula (4)]. Figure 5, which depicts this dependence for three rotational stacks of the ^{4}He – CO and *para*H$_2$ – CO complexes, clearly shows that $E \sim l(l+1)$ with very similar constants of proportionality. Thus, all three features characteristic of nearly free rotations of a monomer manifest themselves in the arrangement of the energy levels of these complexes. [6]

It goes without saying that the above qualitative treatment cannot replace rigorous quantum-mechanical calculations. A thorough description of a method by which such calculations can be carried out was given in Ref. [24]. The calculated energy levels of ^{4}He – CO coincided with the experimental data to within 0.01 cm^{-1} in the case of a semiempirically constructed potential representing the interaction of ^{4}He and CO [22], and to within 0.05 cm^{-1} in the case of an *ab initio* interaction potential [42]. For the *para*H$_2$ – CO complex, such calculations were done by Jankowski and Szalewicz [55, 56].

Thus, with X – CO one can clearly see the transformation of the spectra from the rigid rotation of a complex as a single whole to nearly free rotations of a monomer in He – CO and *para*H$_2$ – CO. However, the alterations in the arrangement of the energy levels caused by such a transformation are quantitative rather than qualitative. More interesting is the case where both monomers rotate, since the addition of their angular momenta leads to dramatic transformations of the spectra.

3.3 Complexes in which both monomers rotate (*para*N$_2$ – CO and CO – CO)

Unfortunately, there has been no serious study of the structure of energy levels of complexes in which both monomers are able to rotate. For this reason, one is forced to focus upon semiempirical considerations. Xia et al. [45] were the first to discover such rotations in *para*N$_2$ – CO. As noted earlier, the N$_2$ molecule in this complex has an intrinsic angular momentum $j_{N_2} = 1$, with the result that already the structure of the lowest energy levels is determined by the addition of rotations of N$_2$ and the complex as a whole. [7] As a result, three stacks emerge (one with $K = 0$, and two with $K = 1$), each consisting of closely spaced levels corresponding to different projections of j_{N_2} on the intermolecular axis.

Figure 6 depicts a diagram of the rotational levels, determined through experiments, of *para*N$_2$ – CO in the ground state (a) and upon excitation of CO vibrations (b). The cornerstone in this diagram was 'laid' by the work of Xu and Jäger [47], who were the first to identify the spectra of the complex in the centimeter wave range and to show that the lower rotational state indeed contains three closely spaced stacks. The arrows in Fig. 6 indicate the spectral transitions by which the levels were determined. Clearly, the spectrum incorporates three parallel R-branches (rotational transitions

[6] Nearly free rotations of a monomer have also been observed in the He – HCN complex [60].

[7] The levels with $j_{N_2} = 3$ are not populated at temperatures maintained in the experiment and no transitions beginning at these levels are observed.

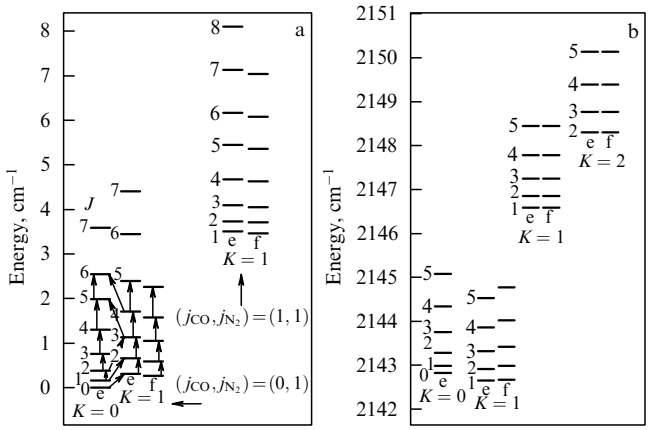

Figure 6. Diagram of the rotational levels of *para*N_2–CO in the ground (a) [47, 58] and vibrationally excited (b) [45] states. The arrows indicate the transitions measured by Xu and Jäger [47].

with $\Delta J = +1$ within each stack). These branches can be identified fairly easily, since the constituent transitions are equidistant in the first approximation: $E(J+1) - E(J) \approx 2hB(J+1)$. What is more important, however, is that the R- and P-branches of transitions between different stacks were also discovered (slanted arrows in Fig. 6). As a result, the same levels are 'connected' by different transition chains, and one can compare the difference in their energies calculated along different chains. [8] And since the accuracy of determining the transition frequencies is very high ($\Delta\nu/\nu < 5 \times 10^{-7}$), the probability of accidental coincidence is very small. Thus, there can be no doubt that the $K = 0$ and $K = 1_e$ rotational levels of stacks have been determined correctly. The situation with the 1_f state is more complicated, since so far no crossed transitions ending on this stack have been discovered, and according to Xu and Jäger [47] the situation remains unclear.

The energy of the 1_f stack was found by Xia et al. [45]. They measured the spectrum of the complex in the IR range and found that this stack lies below 1_e, but above 0_e. It should be noted that the researchers also identified the spectral lines by the combination difference method on the basis of the rotational energy levels determined by Xu and Jäger [47]. Xia et al. [45] obtained the rotational levels of a complex with an excited vibration of CO as well (Fig. 6b), while the levels in Fig. 6a not linked by arrows have been obtained from the spectra taken in the millimeter wave range [58]. It is interesting that as the fundamental vibration of CO is excited, the $K = 1$ stacks prove to be lower in energy than $K = 0$ ones. This means that the states with $K = 0$ and $K = 1$ differ only in the projection of the angular momentum j_{N_2} of the N_2 molecule on the intermolecular axis.

The situation becomes even more interesting when CO rotation is excited. Since $K = j_{N_2} + j_{CO}$, already at $j_{CO} = 1$ there appear nine rotational states separated from the ground state by a small gap $b_{CO} j_{CO}(j_{CO} + 1)$:

$$(j, j) = \begin{cases} (\pm 1, \mp 1), & (0, 0), & K = 0\,, \\ (\pm 1, 0), & (0, \pm 1), & K = 1\,, \\ (\pm 1, \pm 1), & & K = 2\,. \end{cases} \tag{8}$$

Here, one can expect the emergence of many rotational states with close energies. Some of these were discovered upon identification of the spectra of the complex in the IR [45] and millimeter wave [58] ranges. In the upper part of Fig. 6b, where rotational levels of the excited vibrational state are depicted, two groups of pair states with $K = 1$ and $K = 2$ are of special interest. They differ in energy only by 1.5 cm^{-1}, although in rotations of a rigid rotor the energy of the $K = 2$ levels should have been four times higher than that of $K = 1$ ($E \sim K^2$). But if these states correspond to rotations of both CO and N_2 with angular momentum 1, their energies should be on the order of $2b_{CO} = 3.8$ cm^{-1}, as revealed in real situations. So far only levels similar to $K = 1$ states have been discovered in the ground state of the complex ($\nu_{CO} = 0$), but identification of the spectra continues. A fuller set of such states has been found to exist in the CO dimer, and we turn to the description of the spectra of this dimer.

Despite its apparent simplicity, the CO dimer has proved to be one of the most complex objects in molecular spectroscopy, and the identification of its spectrum took about a quarter of a century. It comes as no surprise that the first works in the spectroscopy of this complex were published without any identification of the discovered spectral transitions or with wrong identification [61–63]. Already the first calculations showed that the potential energy of the complex contains several local minima separated by low (≈ 10 cm^{-1}) barriers, with the result that two stable states of different shapes are possible (shape isotopomers) [64]. In one of these the carbon atoms are closer to each other (C-bound), while in the other this is true of the oxygen atoms (O-bound).

What is more, because of symmetry restrictions imposed on the permutation out of identical monomers, the rotational wave functions should transform either by the A^+ representation (if the vibrational wave function is even) or by the A^- representation (if the vibrational wave function is odd) of the C_{2h} group. [9] The gap between the energy levels with these wave functions is about 3.5 cm^{-1} [64]. Only levels with even J in the e-stacks and odd J in the f-stacks satisfy the A^+ representation (with A^-, the situation is just the opposite). Since the inertia tensor of the dimer corresponds to a strongly prolate, slightly asymmetric top molecule and the K-splitting is small, we can think of the sets of K_e and K_f levels (at $K \neq 0$) as residing a single state. Thus, the set of rotational levels exhibiting A^+/A^- symmetry incorporate states with $K = 0$ and even/odd J as well as half of the $K \neq 0$ states (with a complete set of J).

Electrodipole transitions are possible between A^+- and A^--symmetry states. Hence, rotational transitions ($\Delta J = 1$ and $\Delta K = 0$) within a single state are lacking, but the millimeter wave spectrum is extremely dense and has no distinctive structural features.

Shape isotopomers were discovered in the process of identifying the IR spectrum of the CO dimer (in the region of the fundamental vibration of CO) [65]. In these experiments, the researchers resorted to a gas jet at $T \approx 3$ K, so that only transitions from the lower levels of the ground state were measured, and the spectrum became much simpler.

Four stacks of levels [10] with $K = 0$ (a, c) and $K = 1$ (b, d) have been discovered in the ground state of the complex. These correspond to two shape isotopomers with chemical bonds between the monomers that are 0.44-nm long (a, b)

[8] This procedure constitutes the essence of the combination difference method.

[9] This is true for the spinless $(^{12}C^{16}O)_2$ complex. In $(^{13}C^{16}O)_2$, the representations B^+ and B^- are added, but this does not dramatically alter the energy level diagram.

[10] According to tradition which began with Tang et al. [67], the stacks of levels of the CO dimer are denoted by lower-case Roman characters.

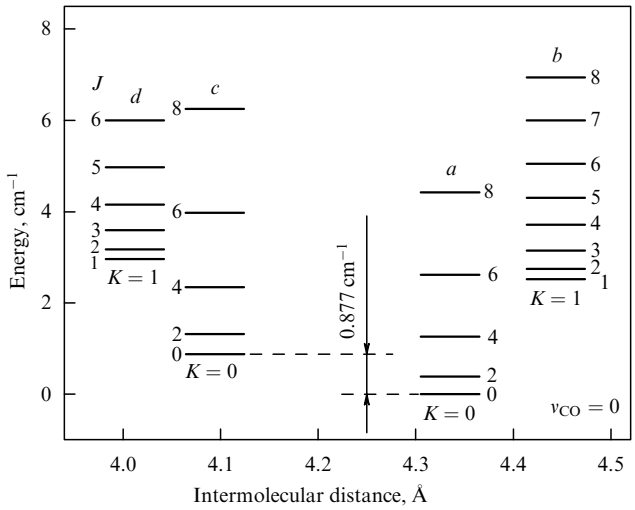

Figure 7. Diagram of the lower rotational levels of the CO dimer [65].

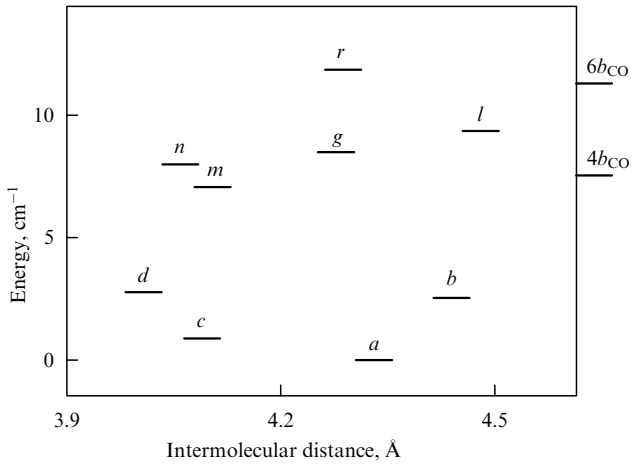

Figure 8. Diagram of the rotational stacks of A^+ symmetry for the CO dimer [68].

and 0.40-nm long (c, d). Altogether, 23 rotational levels with $J = 0, \ldots, 8$ have been revealed (Fig. 7). From the results of the calculations done by Bunker et al. [64] it follows that the intermolecular distance R of the isotopomer with closely spaced oxygen atoms (O-bound) is 0.40 nm, while that of the isotopomer with closely spaced carbon atoms (C-bound) is 0.45 nm. The C-bound isotopomer possesses a lower energy (the difference is only 0.8 cm^{-1}), although according to calculations the energy of the O-bound isotopomer is lower by 10 cm^{-1}. All discovered levels are characterized by the A^+ symmetry.

Following these works, there began a systematic study and interpretation of the millimeter wave spectrum of the CO dimer. What makes this spectrum so specific is that the intensity of transitions between the isotopomers is not much lower than that of transitions within the isotopomers. Hence, all possible spectrum branches (P, Q, R) corresponding to the selection rules $\Delta J = 0, \pm 1$ and $A^+ \leftrightarrow A^-$ occur. About 600 spectral lines in the 80 – 180-GHz range have been discovered in the normal isotopomer $(^{12}C^{16}O)_2$.

Identification of the transitions was made by the combination difference method on the basis of the energies of the known levels. A computer program automatically selected pairs of transitions whose difference between (or sum of) frequencies was equal to the difference between the energies of the known levels, and calculated the energy of a new level. As a rule, the level was assumed found when three transitions associated with it were identified, the transitions such that the calculated energies coincided to within 100 kHz. The selection rules known for dipole radiation were utilized to determine the angular momentum and the parity of the new level and to calculate the frequencies of the other transitions involving this level. If these frequencies landed in the spectrometer's working range, they were searched for. The new levels determined by this procedure were involved in further analysis.

The temperature dependence of the line intensities was also taken into account in the analysis, which made it possible to estimate the energy of the level from which the transition began. The validity of the transition identification procedure was verified by the double microwave – millimeter wave resonance method [19], and the intermediate results have been published in Refs [66 – 68].

All this made it possible to identify 360 transitions and to determine (or clarify) the positions of one hundred levels in the energy range extending to 18.95 cm^{-1} in relation to the lowest energy level of the $(^{12}C^{16}O)_2$ dimer, with the angular momentum J of these levels ranging from 0 to 10 and its projections $K = 0$, 1, 2 on the complex's axis. The energy levels are gathered in to nine stacks with symmetry A^+, and eight stacks of symmetry A^-. The energy of the levels in each stack is reasonably well described by a polynomial expansion of type (7).

Formula (1) is applied with the values of rotational constants B_i to calculate the distance between the monomers that is characteristic of the stack i. Figure 8 shows the initial energies σ_i and the effective intermolecular distances for all A^+-symmetric states of the $^{12}C^{16}O$ dimer. Knowing the intermolecular distances and the characteristic energies, we can easily find that the states $a\,(K = 0)$, b $(K = 1)$, and l $(K = 2)$ belong to the C-bound isotopomer, while the states $c\,(K = 0)$ and $d\,(K = 1)$ belong to the O-bound isotopomer. But there are four more states with intermediate distances between the monomers, with the energies of the states m $(K = 0)$, g $(K = 1)$, and n $(K = 2)$ being close and equal to about 8 cm^{-1}. The reader will recall that in the rigid-rotor model the difference in the energies of the states with $K = 2$ and $K = 0$ should be $\Delta E \approx 4b_{CO} = 7.68$ cm^{-1}. Therefore, it is reasonable to attribute these states to nearly free rotations of both monomers with $j = 1$, with the energy equal to $4b_{CO}$. As mentioned earlier, there should be nine such states. But in the $^{12}C^{16}O$ dimer the states with $K \neq 0$ are double. Here, it may well be that in view of the symmetry of the complex, all combinations $(j, j) = (\pm 1, 0)$, $(0, \mp 1)$ with $K = 1$ are degenerate, as well as those with $K = 0$: $(j, j) = (+1, -1)$ and $(-1, +1)$. In this case, the set $(j, j) = (1, 1)$ of the $^{12}C^{16}O$ dimer should include one state with $K = 2$, one state with $K = 1$, and two states with $K = 0$. The stack r may prove to be the missing state with $K = 0$.

On the other hand, it is quite possible that transitions into certain states are suppressed and the stack r may represent a valence (or stretching) vibration. For instance, the energy of valence vibrations of the Ar – CO complex (close in binding energy) amounts to 18 cm^{-1} [69], which is close to $\sigma_r = 12$ cm^{-1}. Clarifying this problem requires doing additional calculations of the spectrum related to the high-lying levels of the CO dimer.

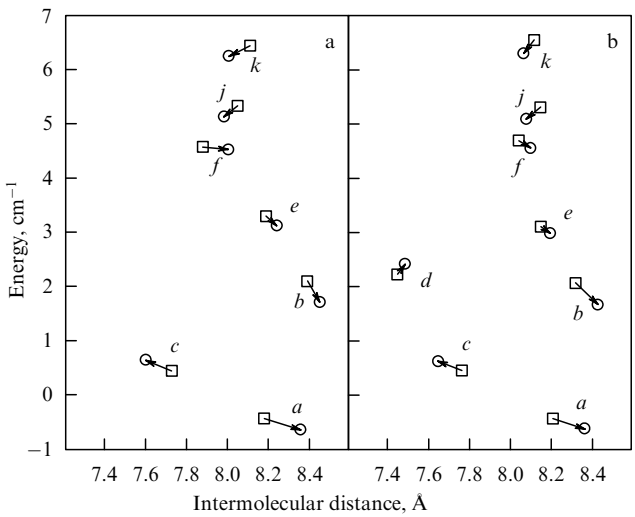

Figure 9. Transformation of the initial energies and effective intermolecular distances of the rotational stacks of the CO dimer in isotopic substitution: (a) experiment [61, 67], and (b) theory [70]: □ — $(^{12}C^{16}O)_2$, ○ — $(^{13}C^{16}O)_2$.

The most recent calculations done by Vissers et al. [70] showed that the A^--states constitute a nontrivial bending vibration of the dimer and not (as assumed earlier) the upper tunnel-splitting components. The researchers were able to fit the CO – CO pair interaction potential such that it described correctly the energies of the lower states of both isotopomers. As a result, they not only were able to achieve rather good agreement with the positions of the experimentally determined energy levels of the $^{12}C^{16}O$ dimers (calculations were done up to energies of about 8 cm^{-1}) but also described the isotope shift of levels in the $^{13}C^{16}O$ dimer, determined in Ref. [71] (Fig. 9).

With respect to the manifestations of intrinsic rotations, the *ortho*H_2 – CO complex is an equally nontrivial system, but its spectra are still being identified.

Thus, for the first time complexes consisting of two molecules, in which both molecules rotate (with intrinsic angular momentum $j = 1$) and the projection of the total angular momentum on the complex's axis is determined by the vector sum of j, were disclosed. It is quite possible that a complete set of these states was discovered in the CO dimer. Even more interesting rotations have been revealed in systems with a large number of helium atoms or hydrogen molecules. We will now discuss experiments involving such systems.

4. Partial entrainment of helium atoms in chromophore rotation. Spectroscopy of the He_N – X (X = OCS, N_2O, CO_2, and CO) nanoclusters in a supersonic gas jet

As the techniques associated with supersonic jets became more sophisticated, the gas cooling became more effective and, accordingly, bigger clusters were produced. As a result, several He_N – X type composites, where X is the light chromophore molecule, have been studied. This research was done by the same groups of A R W McKellar and W Jäger, who utilized the same facilities. [11]

To succeed in these experiments it is important to bear in mind that, because of the high spectral resolution, the spectral lines belonging to different clusters do not overlap and are analyzed separately. Moreover, and this is rather important, the optimum temperature for cluster formation monotonically decreases as the clusters become larger. Hence, as the temperature drops (this is usually done by increasing the initial pressure of the gas), the intensities of the spectral lines pass through a maximum. Its position can be used to assign a spectral line to a cluster of a certain composition. Several such clusters have been studied: He_N – OCS ($N \leqslant 8$) [4, 72, 73], He_N – CO_2 ($N \leqslant 17$) [74, 75], He_N – N_2O ($N \leqslant 14$) [76], and He_N – CO ($N \leqslant 20$) [59, 77]. [12] The shape of all triatomic chromophore molecules is linear and the properties of helium clusters based on them are in many respects similar, so for the sake of convenience we examine them together.

Experiments have shown and calculations have corroborated [74, 79 – 82] that the first five helium atoms in these clusters form a ring in the equatorial plane of the chromophore. This means that beginning with $N = 3$ the inertia tensor of the complex is that of a symmetric top molecule, so that transitions with $\Delta K = 1$ are forbidden and the spectra are fairly simple. In the centimeter wave range, purely rotational transitions with $\Delta J = +1$ (the R-branch) are detected, while in the IR range the transitions with chromophore vibrational excitation $v = 0 \to 1$ and $\Delta J = \pm 1$ (R- and P-branches) are measured. There should also be a Q-branch ($\Delta J = 0$) for these transitions, which links levels with $K > 0$. But at the temperatures considered these states are not populated and no Q-branches have been observed in large clusters. [13] The energies of the levels involved in the transitions are described fairly well by polynomials [see formula (7)] where in the ground (lower) state $\sigma_i = 0$, and in the upper state σ_i is the chromophore molecule's vibration frequency. The number of measured transitions is sufficiently large to be able to determine from the spectral lines the first coefficients in polynomial (7), i.e., the rotational constant B, the value of the centrifugal distortion D, and the shift Δv of the fundamental vibration frequency in relation to the frequency of a free molecule. These characteristics of clusters based on all three molecules are depicted in Fig. 10 as a function of the number of attached helium atoms [75].

All the experimental data correlates well with the model in which the first five helium atoms form a rigid ring in the equatorial plane of the cluster. The atoms in this ring do not vibrate together with the chromophore, but they somewhat increase the rigidity of the cluster because of van der Waals attraction, and the fundamental vibration frequency rises linearly with the number of attached helium atoms up to $N = 5$. The next atoms arrange themselves on the periphery of the cluster and contribute substantially to the vibrating mass. Accordingly, the frequency shift changes sign. The fact that the centrifugal distortion for a cluster containing five helium atoms has a minimum is also an indication that this configuration possesses maximum rigidity.

Quantitatively, the model is verified most reliably by the behavior of the cluster's inertia tensor. Indeed, the N-dependences of the rotational constant up to $N = 5$, calculated in the equatorial-ring geometry, are in good agreement with the measurement data.

[11] Today our group [9] is also in close collaboration with them.

[12] In addition, the He_N – HCCCN cluster ($N \leqslant 16$) has been studied in the microwave range, but so far only a report has been presented [78]. In a time of preparing this review for the press, the study of the He_N – N_2O system has been brought to $N = 19$ [111].

[13] We will return to this problem when discussing clusters with hydrogen.

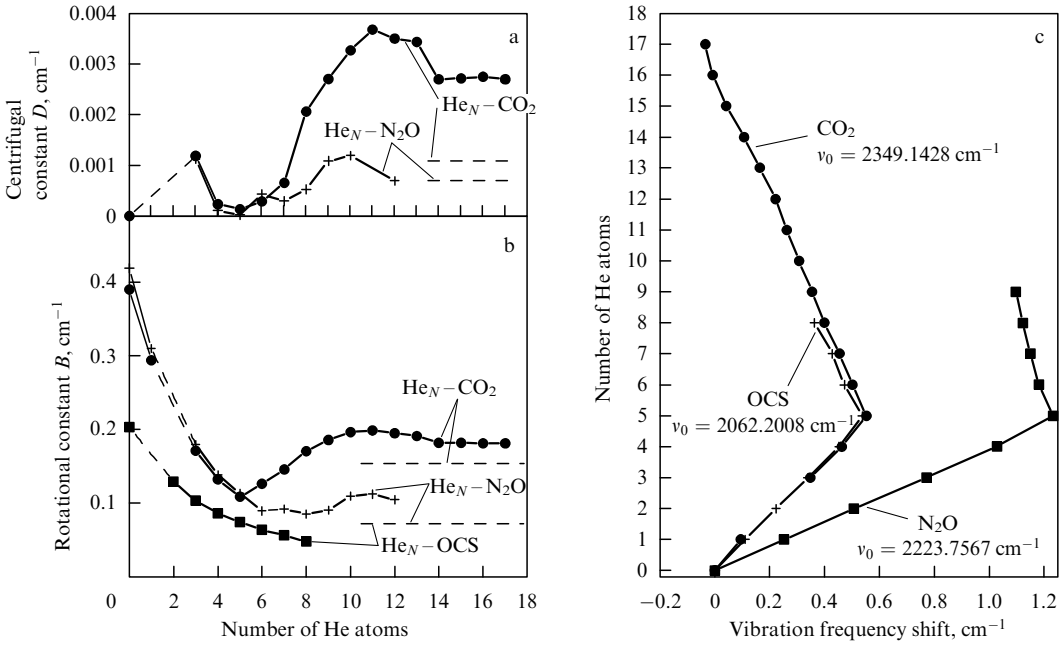

Figure 10. The centrifugal constant D (a), the rotational constant B (b), and the shift in vibration frequency (c) as functions of the number N of helium atoms in He_N-X clusters [75].

Marked differences begin as more helium atoms are attached. In clusters with OCS molecules, the rotational constant continues to decrease with a somewhat lower rate. Calculations done by Moroni et al. [79] show that such behavior is caused by the formation of a second ring of helium atoms near the oxygen atom. In clusters with N_2O molecules, the constant B changes only slightly as the number of attached atoms is increased (a small maximum is observed at $N = 10-11$), while in compounds with CO_2 molecules it begins to smoothly growth and reaches its maximum value at $N = 11$. Here, the growth is substantial, so that the rotational constant of a cluster with 11 helium atoms is greater (the moment of inertia is smaller) than in a cluster with three atoms. These results indicate that the chromophore molecule rotation in rather large clusters is accompanied by only the partial entrainment of attached helium atoms. Within the accuracy of experimental study, this motion is nondissipative, since no additional broadening of the spectral lines has been observed.

It is interesting to compare these results with the rotations of the same molecules in helium nanodroplets [83] (the horizontal lines in Fig. 10). The rotational constants of OCS molecules in nanodroplets and in a cluster with five helium atoms are almost the same. It is natural to assume, then, that when this molecule is dissolved in helium it also forms a ring of five helium atoms surrounding it. For CO_2 molecules embedded in nanodroplets, the value of the rotational constant is between its values in clusters with three and four atoms, which points to a considerable deformation of the ring caused by the interaction with the environment. The rotational constants of all the N_2O-based clusters studied so far are larger than in the case of a nanodroplet. Generally, as the calculations done by Tang et al. [74] and the most recent experiments with large OCS clusters [84] show, the values of the rotational constants increase with cluster size but do not reach the saturation plateau very fast.

The most interesting results have been obtained for CO-based helium clusters. It should be immediately noted that the binding energy of a CO molecule and a helium atom is very low[14] (9 K) and is close to the chemical potential of liquid helium. The spectra of the clusters were measured by McKellar's group in the IR range near the CO fundamental vibration frequency (2143 cm^{-1}), and the results have been published in Ref. [59] for $^{12}C^{16}O$, and in Ref. [77] for $^{13}C^{16}O$ and $^{12}C^{18}O$. Since the formation of these clusters requires using very low temperatures (0.1 – 0.3 K), only the lowest energy level with $J = 0$ is actually populated, so that basically transitions from this level, R(0), were measured. However, in contrast to other clusters, here the researchers were able to observe not only transitions with $\Delta K = 0$, which excite the rotation of the chromophore together with the cluster, but also transitions with $\Delta K = 1$, which excite a nearly free rotation of CO. Similar transitions in the He – CO rotational spectrum were reflected in Fig. 4. In IR spectra, the CO vibration is added to these. The measured transition frequencies are depicted in Fig. 11 as functions of the number of helium atoms in a cluster.

Two features of molecular rotations in these clusters are clearly visible. First, the frequencies of transitions with $\Delta K = 0$ (the left branch in Fig. 11) in small clusters decreases much more slowly than in the case of triatomic molecules, and already at $N = 3$, 4 the value of the rotational constant B greatly exceeds the one expected for the case of rigid rotation of the entire cluster. Then the frequency of this transition increases significantly and approaches the value of the R(0) transition frequency for a free molecule. In other words, the CO molecule in such a cluster rotates almost freely. At $N = 15$ there is observed anomalous splitting of the transition line into two components. As the cluster gets bigger, the R(0) transition frequency decreases slightly and approaches the value measured in helium nanodroplets [86] (the dashed line in Fig. 11).

[14] This follows from the measured dissociation energy of He – Co [5] and from the calculations done by Cazzato et al. [85].

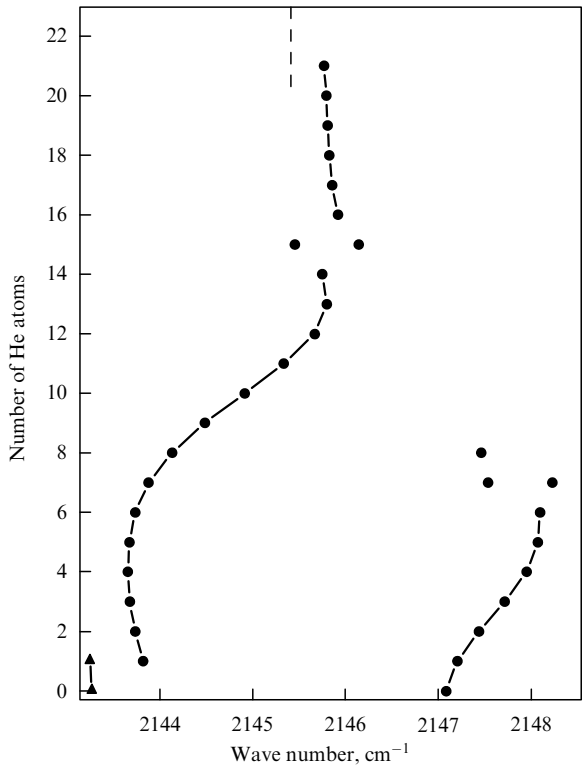

Figure 11. The transition frequencies $\nu_{CO} = 1-0$, R(0) $\Delta K = 0$ (left branch) and R(0) $\Delta K = 1$ (right branch) in He_N-CO: ▲, the value of the transition frequency obtained by Tang and McKellar [59]; – – –, the transition frequency $\nu_{CO} = 1-0$, R(0) $\Delta K = 0$ in helium nanodroplets [86].

The other feature is related to the frequency of transitions with $\Delta K = 1$ (the right branch in Fig. 11). As noted earlier, already in He–CO the frequency of such a transition exceeds $2b_{CO}$. The transition frequency continues to grow as new helium atoms are added and passes through a maximum at $N = 7$ (in such a cluster the line splits). [15] The decrease in the frequency of transitions with $\Delta K = 1$ in large clusters is better seen in $^{13}C^{16}O$, where it was observed up to $N = 10$ by McKellar [77].

Unfortunately, these data are insufficient if we want to independently determine the rotational constant and the shift in frequency of the CO fundamental vibration in helium clusters. However, this shift is small (0.027 cm^{-1} for He–CO, while the calculated value is $0.05N$ cm^{-1} [85]) and cannot introduce qualitative changes. Furthermore, the rotational transitions with $\Delta K = 0$ and $\Delta K = 1$ for clusters with two and three helium atoms have been measured directly (see Refs [87] and [9], respectively), and the results correlate well with the IR data.

The behavior of the intensity of these transitions is also of interest. As noted earlier, the transitions with $\Delta K = 0$ are forbidden in the model of CO free rotations, and in the He–CO clusters they are weaker than those with $\Delta K = 1$ by a factor of ten. As the clusters become bigger, the intensity is redistributed between these transitions (the intensity of the first increases, and that of the second decreases), and in large clusters the intensities of the transitions with $\Delta K = 1$ fall below the spectrometer's sensitivity threshold.

[15] At present, the reasons for such splitting are unknown.

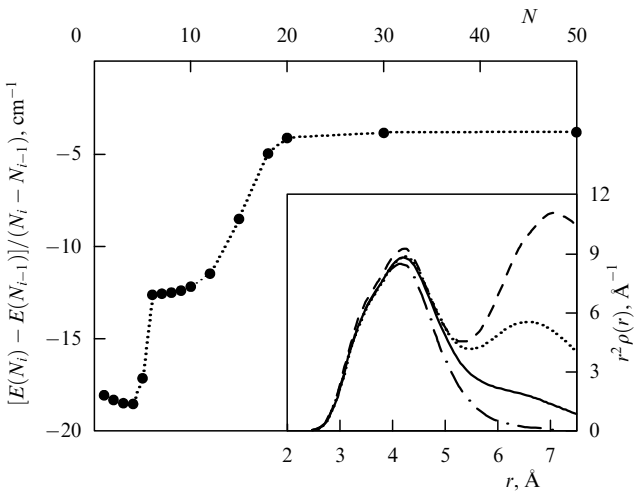

Figure 12. Binding energy per helium atom in He_N-CO_2 as a function of cluster size [74]. The inset shows the radial distribution of the helium atom density at $N = 15$ (dot-and-dash curve), $N = 20$ (solid curve), $N = 30$ (dotted curve), and $N = 50$ (dashed curve).

A computational investigation of these clusters is carried out by the quantum Monte Carlo method based on the pair interaction potentials in He–X and He–He dimers, obtained by *ab initio* calculations or fitted according to the data on the spectra of binary systems. Figure 12 shows the calculated binding energies of helium atoms in a CO_2-based cluster [74]. The first five helium atoms, which form the equatorial ring, are those most rigidly attached to the chromophore. The next helium atoms, with lower binding energies, are diffusely arranged at the periphery of the cluster. A sharp decrease in binding energy between $N = 12$ and $N = 18$ accompanies the filling of the first coordination sphere. This drop in binding energy is illustrated by the inset to Fig. 12, where we have depicted the radial dependence of the helium atom density in the cluster. Helium clusters based on other triatomic molecules are organized in a similar manner.

The dependence of the binding energy of helium atoms on the size of the He_N-CO clusters is less structured [85]. However, in this case, too, calculations of the wave functions reveal that the first six helium atoms form a diffuse ring in the plane perpendicular to the CO-axis; the ring begins to inflate to the poles as additional helium atoms are attached. But due to the mutual attraction of helium atoms, this ring is heavily deformed. Figure 13 demonstrates the probability density of the azimuthal arrangement of two helium atoms. Clearly, the distribution goes through a maximum at $\varphi \approx \pi/3$ even for a cluster consisting of three helium atoms.

Figure 14 shows the calculated frequencies and intensities of rotational transitions with $\Delta K = 0$ and $\Delta K = 1$ in the He_N-CO clusters. The experimental values of the frequencies were obtained by Tang and McKellar [59] taking into account the shift in the CO fundamental vibration frequency, calculated by Cazzato et al. [85]. Clearly, the calculated frequencies in both branches of the spectrum correlate well with the experimental data, except for the splitting of spectral lines observed in some clusters (at present, the reasons for such splitting are unknown). The calculated intensity redistribution also qualitatively agrees with the results of experiments. Zillich et al. [88] also calculated the spectra of the He_N-CO clusters with similar results.

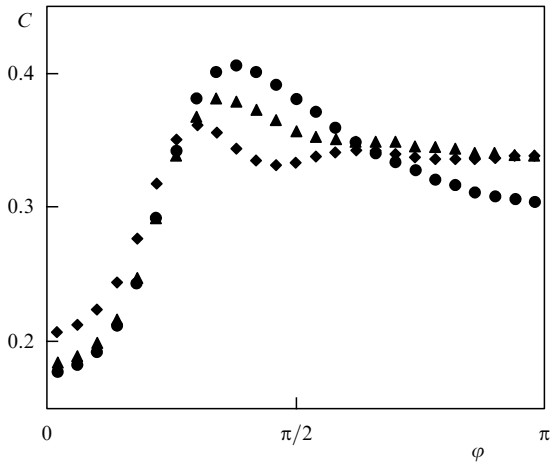

Figure 13. Probability density of the azimuthal arrangement of two helium atoms in He_N-CO when $N = 3$ (●), $N = 6$ (▲), and $N = 9$ (◆) [85].

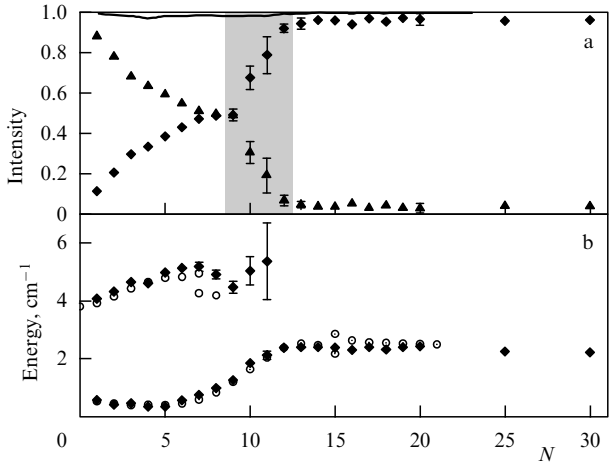

Figure 14. (a) Calculated intensities of R(0) transitions with $\Delta K = 0$ (◆) and $\Delta K = 1$ (▲) in He_N-CO [85]. The curve at the top indicates the total intensity, and the hatched area corresponds to the region with large counting errors. (b) Calculated (◆) and experimental (○) [59] values of the frequencies of rotational transitions R(0) with $\Delta K = 0$ and $\Delta K = 1$ in the He_N-CO clusters [85].

Unfortunately, the physics of the phenomena observed is unclear if one relies on these two papers [85, 88]. However, the following picture may be imagined: only a portion of the entire helium shell is involved in the CO rotation; rather, it is its anisotropic part that is involved, and this explains the deficit of the moment of inertia. As the shell fills with helium atoms, it becomes more homogeneous and the chromophore begins to rotate faster. In a completely filled shell, the CO molecule rotates almost freely. Nevertheless, due to its attraction to the oxygen atom, the shell is slightly deformed, and this deformation accompanies the CO rotation. Hence, the rotation frequency is slightly lower than for a free molecule. More than anything, such rotation resembles a tidal wave on the ocean's surface.

At present there is no qualitative explanation of the rise in the frequency of transitions with $\Delta K = 1$. Its drop in large clusters is easier to explain. States excited by transitions with $\Delta K = 0$ and $\Delta K = 1$ differ in the directions of their rotation axes. When the helium shell is completely filled, separation of two rotations loses all meaning and their frequencies should

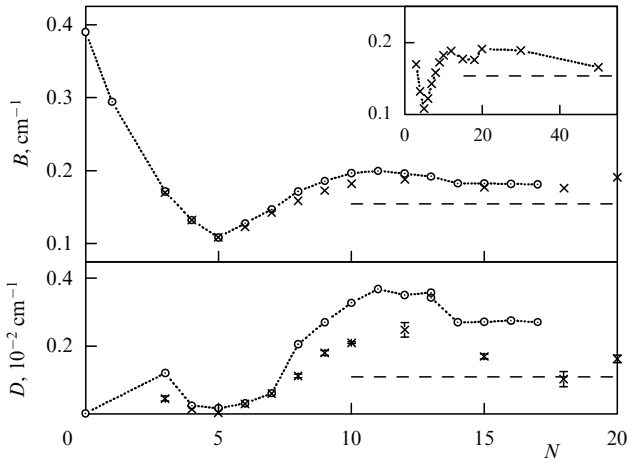

Figure 15. Experimental (circles) and calculated (crosses) values of the rotational constant B and the centrifugal constant D in the He_N-CO_2 clusters [74]. The horizontal dashed lines mark the values found in nanodroplets.

become equal. This also explains the observed redistribution of the transition intensities.

It can be assumed that such phenomena are also characteristic of rotations of large helium clusters based on triatomic molecules. The main difference is that here, for any size of a cluster, the equatorial helium ring accompanies the rotation of the chromophore to a larger (OCS) or lesser (CO_2) degree. The results of spectrum calculations by the quantum Monte Carlo method are in good agreement with the experimental data, which is illustrated by Fig. 15 where the experimental [75] and calculated [74] values of the B and D constants are depicted as functions of the He_N-CO_2 cluster size. Tang et al. [74] also explain the reasons for the differences in behavior of rotations in clusters based on triatomic molecules. The point is that the sixth helium atom in OCS- and N_2O-based clusters is localized at a given end of the molecule and does not hinder the rotation of the ring together with the chromophore. In view of the CO_2 symmetry, here the sixth atom is distributed between the poles and hinders the motion of the ring, which reduces the effective moment of inertia and increases the rotational constant.

Such nondissipative nonuniform rotations do indeed resemble superfluidity phenomenon. We will return to this problem after describing similar experiments with clusters based on molecular hydrogen.

5. Partial entrainment of H_2 molecules in chromophore rotation. Spectroscopy of the $(H_2)_N-X$ (X = OCS, N_2O, and CO) nanoclusters. Comparison with experiments conducted on helium nanodroplets

The heightened interest in studies of nanoclusters based on molecular hydrogen is related to the search for hydrogen superfluidity predicted by V L Ginzburg and A A Sobyanin in 1972. In their paper [89], they showed that liquid parahydrogen could become superfluid at $T \approx 6$ K if it were not for the fact that it freezes at 13.6 K. Subsequent calculations made slight corrections to the value of the transition temperature [90, 91]. Sindzingre et al. [92] predicted that superfluidity can be realized in weakly bound hydrogen nanoclusters. More-

over, there have been reports of superfluidity being detected in hydrogen clusters inside helium nanodroplets [93].

Such research has stimulated the study of hydrogen nanoclusters in supersonic jets. Technically, these experiments resemble those discussed above in connection with the helium nanoclusters. The main difference is that here hydrogen (a diatomic molecular gas) has a smaller adiabatic exponent and its cooling proceeds with greater difficulties. Hence, the original gas mixture consisted of helium with 1% hydrogen molecules and 0.1% chromophore. As a result, temperatures close to that of a purely helium jet have been attained, but the hydrogen clusters are mainly produced in view of the higher binding energy of hydrogen molecules with the chromophore.[16] Another characteristic feature is connected with the presence of *para*-modification or *ortho*-modification in the hydrogen molecule. Hence, to separate their spectra, the hydrogen was pretransformed entirely into nearly pure parahydrogen by using a cryogenic converter.

McKellar's group has studied free hydrogen clusters in the IR range. So far three systems have been studied: $(H_2)_N-CO$ with $N = 1-14$ [94], $(H_2)_N-N_2O$ with $N = 1-13$ [95], and $(H_2)_N-OCS$ with $N = 1-7$ [96].

The results of measurements covering the $(H_2)_N-CO$ spectra are close to those obtained for He_N-CO by Tang and McKellar [59]. In exactly the same way, rotational transitions from the lowest energy level with $J = 0$ have been measured. The researchers were able to detect transitions with $\Delta K = 0$ in clusters containing up to 14 hydrogen molecules, and transitions with $\Delta K = 1$ in clusters containing up to 8 hydrogen molecules. As the clusters become bigger, the intensity of the former increases, while that of the latter decreases and becomes lower than the spectrometer's sensitivity threshold. Similar to He–CO clusters, the former transitions excite CO rotation together with the cluster, while the latter excite free chromophore rotation. What is more, in clusters with $N = 2-5$ the researchers discovered R(1) transitions to the levels with $J = 2$ and $K = 1$. To determine the frequencies of the rotational transitions one should know the shift in the fundamental vibration frequency in clusters with different compositions. By analogy with helium clusters, this shift was assumed to be linear: $\Delta\nu = \alpha N$ (where $\alpha = -0.18\ \mathrm{cm}^{-1}$) is the shift of the frequency in *para*H_2–CO [6]. Figure 16 shows the frequencies of rotational transitions obtained through experiments together with the results of theoretical evaluations.

In contrast to helium clusters, here the frequency of $\Delta K = 1$ transitions begins to rise at $N = 5$, while that of transitions with $\Delta K = 0$ begins to rise at $N = 7$. The frequency of $\Delta K = 0$ transitions increases rather rapidly and at $N = 10$ reaches its maximum ($3.35\ \mathrm{cm}^{-1}$), which amounts to 85% of the frequency of this transition in the CO molecule and is larger than the value obtained for helium clusters. The frequency of the $\Delta K = 1$ transition at a maximum (with $N = 7$) is almost 1.5 times larger than the rotation frequency of a free CO molecule. The spectral lines in $(H_2)_N-CO$ exhibit no anomalous splitting.

Calculations of the spectra of hydrogen clusters were done by the same method as that used for helium-based clusters. In Fig. 16, the results of such calculations are shown by black circles. The lower branch (the rotation of the cluster as a whole) fits very well the experimental values, while the calculated frequencies of the CO rotation with respect to the cluster even noticeably exceed these values. Thus, the rotation of $(H_2)_N-CO$ clusters is also accompanied by partial entrainment of the cloud of hydrogen molecules, which leads to an increase in the transition frequency (a decrease in the cluster's inertia tensor) with cluster size. The amplitude of an increase in the rotation frequency is larger, and this increase begins at a larger cluster size than in the case of helium clusters.

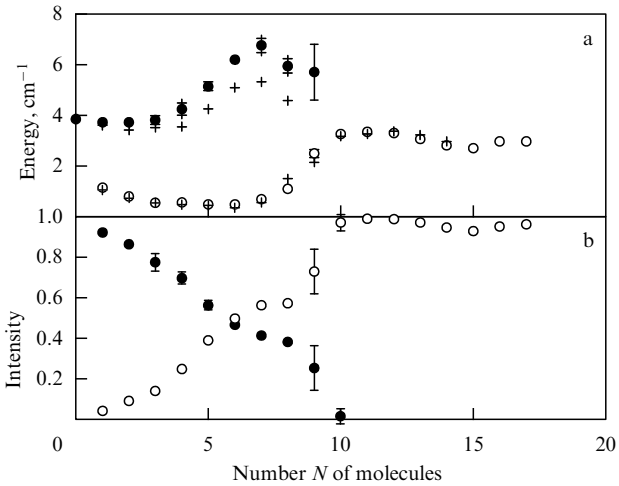

Figure 16. (a) Calculated (●) and experimental (+) frequencies. (b) Intensities of rotational R(0) transitions with $\Delta K = 0$ and $\Delta K = 1$ in the $(H_2)_N-CO$ clusters [94].

The $(H_2)_N-N_2O$ and $(H_2)_N-OCS$ clusters were studied in the IR range near the frequencies ν_1 of fundamental vibrations of chromophore molecules. For $N > 2$, they resemble, just as helium clusters, a symmetric top molecule, and their spectra also have a fairly simple structure (only transitions with $\Delta K = 0$ have been recorded). The number of measured spectral lines is sufficiently large, so that the values of the vibration frequency shift and the rotational constant can be found independently.

In contrast to the case of H_2-CO and N_2-CO complexes, the spectra of clusters of the *para*- and *ortho*-modifications of hydrogen with embedded N_2O molecules have similar structures even for binary systems [97]. Here, the main difference lies in the fact that the $(ortho H_2)_N-N_2O$ cluster exhibits Q-branches of the rotational transitions, while no such branches exist in the $(para H_2)_N-N_2O$ cluster. This phenomenon can be explained by the peculiarities of the structure of the rotational energy levels, which stem from the symmetry requirements imposed on the wave functions by the permutation of identical hydrogen molecules. In view of this, the symmetric configurations of *para*H_2 and ^{4}He (nuclear spin zero) contain only levels with $K = nN$, where N is the number of hydrogen molecules in a ring, and n is an integer. For $N > 2$, these states with $K > 0$ have high energies ($\sim K^2$) and are not populated at the experiment temperatures. Hence, the Q-branch which connects states with equal values of $K \neq 0$ is not observed at all. In $(ortho H_2)_N-N_2O$ there are levels with all values of K (albeit, with different statistical weights). The level with $K = 1$ has a fairly low energy and is populated at the temperatures of the experiment.

Figure 17 depicts the shift in the vibration frequency and the rotational constant B as functions of the size of the $(H_2)_N-N_2O$ cluster. In exactly the same way as in helium

[16] For instance, the binding energy in CO-based clusters amounts to 9 K per helium atom, and is about 30 K per hydrogen molecule.

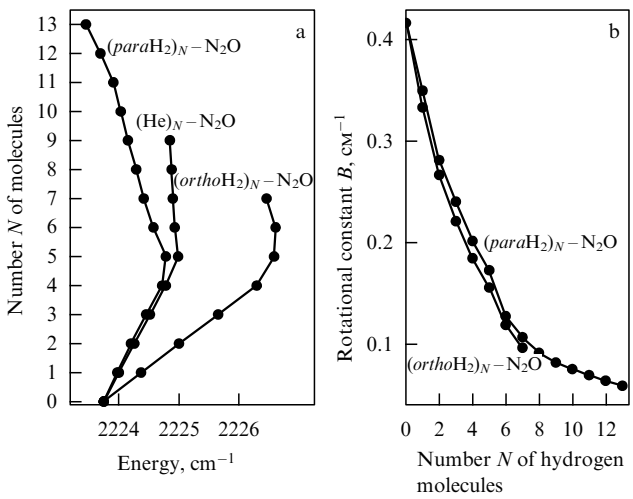

Figure 17. (a) Vibration frequency shift, and (b) the rotational constant B in the $(H_2)_N - N_2O$ clusters [95].

clusters, the vibration frequency shift has a knee at $N = 5$, which points to the formation of a ring consisting of five hydrogen molecules in the equatorial plane. The stability of this configuration in OCS-based hydrogen clusters has been corroborated by the results of calculations done by Paesani et al. [98]. The main difference in behavior is that the rotational constant B for $N > 5$ does not become saturated; instead, it continues to decrease. It may be assumed that due to the higher binding energy the $(para H_2)_N - N_2O$ cluster rotates as a whole up to $N = 13$.

What makes OCS-based hydrogen clusters so interesting is that their absorption spectra have been measured both in a free state [96] and in helium nanodroplets [93, 99, 100]. Unfortunately, Tang and McKellar [96] were able to identify the spectra of clusters containing only up to seven $para H_2$ molecules and six $ortho H_2$ and HD molecules. Figure 18 shows the dependences of the rotational constants and the vibration frequency shifts on cluster size. The results for all three modifications of hydrogen are similar to each other and are close to the data on helium clusters. The knees in the

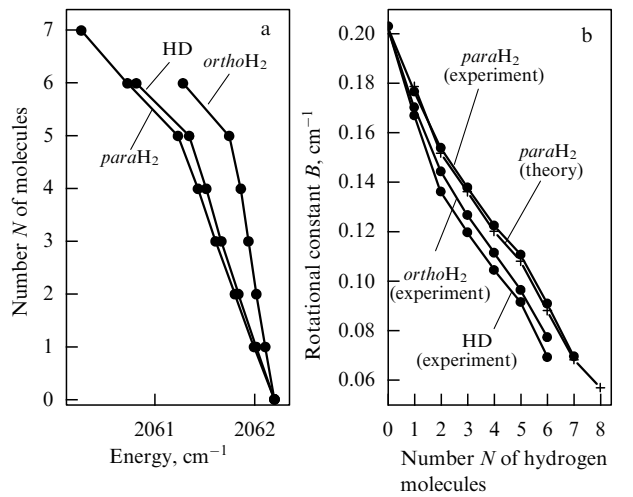

Figure 18. (a) Vibration frequency shift, and (b) the rotational constant B in the $(para H_2)_N - OCS$, $(ortho H_2)_N - OCS$, and $(HD)_N - OCS$ clusters [96]. The crosses indicate the results of calculations for $(para H_2)_N - OCS$ [98].

diagrams at $N = 5$ also point to the stability of the configuration with five attached hydrogen molecules. The behavior of the rotational constant is in good agreement with the results of calculations of the structure and the inertia tensor of the cluster made by Paesani et al. [98] (the crosses in Fig. 18b), i.e., as in helium clusters of the same composition, no deficit in the moment of inertia is observed and the cluster rotates like a rigid rotor.

Just as in N_2O-based clusters, all three branches of the rotational transitions [R ($\Delta J = 1$), P ($\Delta J = -1$), and Q ($\Delta J = 0$)] are observed in the $(ortho H_2)_N - OCS$ and $(HD)_N - OCS$ clusters, while in the $(para H_2)_N - OCS$ and $He_N - OCS$ clusters there is no Q-branch. It is also important to emphasize that no significant differences in the properties of clusters involving HD Fermi particles have been revealed.

Thus, rotations with slippage (with a deficit in the moment of inertia) of molecular hydrogen set in at cluster sizes larger than in the case of helium, and so far have been observed only in $(para H_2)_N - CO$. This effect can be attributed to the higher binding energies of hydrogen molecules and chromophores.

The development of techniques of handling with helium nanodroplets made it possible to dope such nanodroplets not only with individual molecules but also with entire aggregates of a different composition. And since the dopants are bound to each other more strongly than to the surrounding helium, a cluster with embedded molecules forms inside a nanodroplet. The $(H_2)_N - OCS$ clusters were produced in exactly this way, and their properties were studied by the absorption spectra near the OCS fundamental vibration frequency.

The binary system X – OCS, where X = H_2, HD, and D_2, is the most studied one [99]. In this composition, the rotational spectrum is well-resolved and consists of a sufficiently large number of lines for the analysis to be successful. All three rotational constants have been determined for all compositions, both in the ground state and in a vibrationally excited state. The main result implies that the rotational constants are much smaller than those for a free complex. For instance, the A constant is nine times smaller, while B and C are three times smaller.

Grebenev et al. [100] studied the rotational constants for the $(para H_2)_N - OCS$ and $(ortho D_2)_N - OCS$ clusters with $N = 2-8$ as functions of the cluster composition. In contrast to free clusters, the experimental spectra at $N = 2-4$ are described much better by the asymmetric-top model ($B \neq C$). Accordingly, Q-branches are observed even in $para H_2$ clusters. Their intensities were used to estimate the I_a component of the inertia tensor. The dependences of all the tensor components on the cluster size are given in Fig. 19. Clearly, they gradually increase with the number of attached molecules, with the exception of the rapid decrease of I_a in $(para H_2)_N - OCS$ at $N = 5$, 6. There are no Q-branches in these clusters, and the values listed in the diagram were obtained on the assumption that the levels with $K = 1$ rise above the thermal energy.

This feature can also be explained by the fact that the most rigid configuration of a filled ring is achieved in clusters with five or six hydrogen molecules and that there is no reduction in the symmetry of such a configuration because of the interaction of the hydrogen molecules with the surrounding helium. In this case, just as in a free cluster, there are only levels with values of K that are integral multiples of N, and with energies so high that they are not populated at the experiment temperatures.

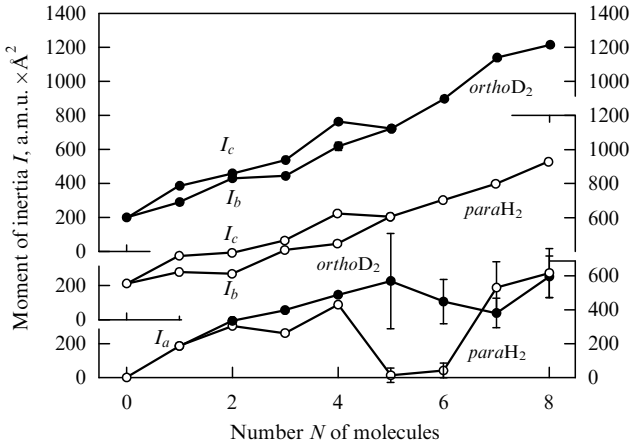

Figure 19. Components of the inertia tensor as functions of the size of the $(para\mathrm{H}_2)_N-\mathrm{OCS}$ and $(ortho\mathrm{D}_2)_N-\mathrm{OCS}$ clusters in helium nanodroplets [100].

It may be assumed that the structure of the heavier clusters is not as rigid, that the surrounding helium breaks the cylindrical symmetry, and that Q-branches again appear. The absence of noticeable differences between the transverse components of the inertia tensor is due to insufficient spectral resolution of the spectrometer.

Thus, the surrounding helium not only renormalizes the rotational constants but also lowers the symmetry of the hydrogen clusters. Hence, clusters in helium nanodroplets are independent objects and comparing their properties with those of free clusters of the same composition is highly problematic. Suffice it to note that no decrease in the moment of inertia (acceleration of chromophore rotation) with an increasing number of attached molecules has been discovered in the $(\mathrm{H}_2)_N-\mathrm{OCS}$ clusters in helium nanodroplets.

6. The problem of 'nanoscopic' superfluidity in small helium and hydrogen clusters

Superfluidity of hydrogen dissolved in helium nanodroplets was discovered by Grebenev et al. [93]. The researchers studied the absorption spectra of $(para\mathrm{H}_2)_N-\mathrm{OCS}$ and $(ortho\mathrm{D}_2)_N-\mathrm{OCS}$ within the range of compositions close to the filling of the first hydrogen coordination sphere ($N = 14-17$). The measurements were made in nanodroplets of pure ^{4}He ($T \approx 0.37$ K) and in a ^{3}He/^{4}He mixture ($T \approx 0.15$ K). Figure 20 displays the experimental spectra.

In both types of clusters at 0.37 K, Q-branches (transitions with $\Delta J = 0$) are clearly visible. They disappear in hydrogen clusters as the temperature gets lower, but remain in deuterium clusters. The researchers related this effect to the hydrogen transition at $T = 0.3-0.2$ K to the superfluid state; this transition restores the cylindrical symmetry of the clusters, and, accordingly, the forbiddance of states with $K \neq N$ and the population depletion of levels with $K \neq 0$ (due to their high energy). In deuterium clusters, as mentioned earlier, there is no such forbiddance and superfluidity (if it does set in) nowise manifests itself.

However, a correct interpretation of the discovered effect is hindered by the fact that rotational relaxation in nanodroplets of pure ^{4}He is not only stronger than in an ^{3}He/^{4}He mixture but its frequency is close to the spacing between rotational levels. In view of this, there may be substantial

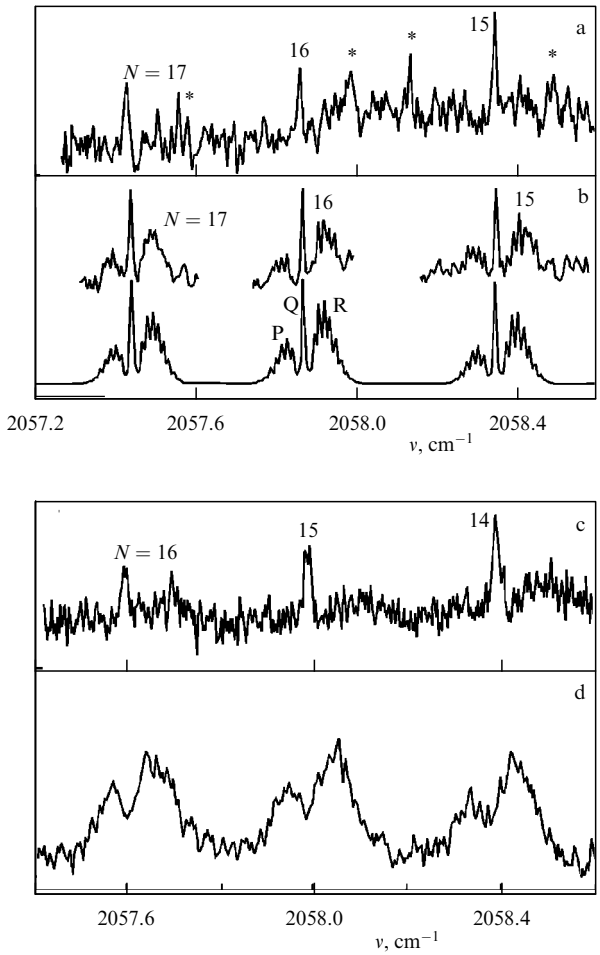

Figure 20. (a) Vibrational spectra of the $(ortho\mathrm{D}_2)_N-\mathrm{OCS}$ clusters in nanodroplets of pure ^{4}He. (b) The same as in an ^{3}He/^{4}He mixture. (c) Vibrational spectra of the $(para\mathrm{H}_2)_N-\mathrm{OCS}$ clusters in nanodroplets of pure ^{4}He. (d) The same as in an ^{3}He/^{4}He mixture [93]. The third spectrum from the top was built on the basis of theoretical predictions.

redistribution of the transition intensities, which leads to a rise in the Q-branch at the expense of the R- and P-branches. Indeed, the R- and P-branches are practically absent in the spectra measured in pure ^{4}He (Fig. 20), while the intensity of the Q-branch may be significantly higher than the equilibrium value. [17] Switching off this effect in nanodroplets produced from an ^{3}He/^{4}He mixture may contribute significantly to a dramatic decrease in the intensity of the Q-branch.

Moreover, in the spinless system the existence of the Q-branch rather than its absence is a nontrivial feature. In small clusters, the appearance of a Q-branch is attributed to the cylindrical symmetry breaking caused by the surrounding helium [100], while no Q-branches have been observed in free clusters of helium or parahydrogen. In large $(para\mathrm{H}_2)_N-\mathrm{OCS}$ clusters, the detected disappearance of Q-branches in the spectrum of OCS vibrations is an interesting fact, but we believe it is still too early to state that we are dealing here with hydrogen superfluidity. [18]

[17] A highly nonequilibrium distribution of the intensities of rotational lines has been recorded, e.g., for the excimer He_2 molecule in superfluid helium [101]. The line broadening in helium nanodroplets has been thoroughly studied in Refs [102, 103].

[18] For instance, Callegari et al. [104] expressed their doubts concerning the relation between this effect and hydrogen superfluidity.

Let us continue, however, with free clusters. In these clusters, the observed rotations with a deficit of moment of inertia (especially in He_N-CO, He_N-CO_2, and $(H_2)_N-CO$) resemble the well-known experiment of Andronikashvili [105], in which the density ρ_s of the superfluid component of helium was determined from the decrease in the moment of inertia of a stack of disks twisting together with the surrounding liquid. This analogy did not go unnoticed, when Paesani et al. [106] calculated the fraction ρ_s/ρ for He_N-CO_2. Since this cluster is anisotropic, the researchers separately calculated the densities of the superfluid ring currents parallel ($\rho_{s\,||}$) and perpendicular ($\rho_{s\,\perp}$) to the CO_2-axis. They found that the effect shows itself not even at six (as could be assumed from the beginning of the increase in the rotational constant) but at five helium atoms, since the filled equatorial ring proves to be superfluid. Similar calculations for the $(para H_2)_N-OCS$ clusters demonstrate that $\rho_{s\,||}$ appears for $N > 9$, and $\rho_{s\,\perp}$ for $N > 13$ [107].

It would seem that these assertions contradict the experimental results obtained by Grebenev et al. [3], who found that there should be no less than 60 atoms for the onset of superfluidity in liquid helium. However, the researchers studied nanodroplets produced from an $^3He/^4He$ mixture and the effect they exposed only means that 60 ^4He atoms are needed, not for superfluidity to set in, but for related separation of the solution of these isotopes. In pure ^4He, superfluidity may set in even with a smaller number of atoms.

Furthermore, recent experiments with free He_N-OCS clusters have moved up to $N = 70$ [84]. As new helium atoms are added to the cluster, the rotational constant B begins to grow and finally reaches a plateau on which small oscillations are superimposed. The maxima in B occur when the coordination spheres are completely filled. Here, no additional spectral line broadening above the Doppler value, i.e., no relaxation, has been detected. Thus, the transition of free helium clusters into the superfluid state occurs smoothly and there is no way (with the exception of the deficit of the moment of inertia) to establish the exact point of manifestation of superfluidity.

Let us not be in a hurry to draw conclusions, however. The calculations of the rotational spectra of these clusters that were done by Tang et al. [74], Cazzato et al. [85], and Moroni et al. [94] shown that the moment of inertia decreases with increasing cluster size even not taking into account the superfluidity effect. The fact that the rotations in these clusters are nondissipative may be explained by the absence of a thermal reservoir in such small systems. Hence, the question of whether there is superfluidity in such systems may be resolved only through experiments in which the properties of clusters produced from Bose and Fermi particles (^3He and HD) are compared. [19]

Unfortunately, these isotopes are quite expensive, and we know of only one experiment with fermionic systems, conducted by Moore and Miller [108], in which the behavior of the $(HD)_N-HCN$ clusters in helium nanodroplets was investigated. The researchers studied the HCN vibrations near 3300 cm^{-1} within a broad range of HD concentrations and identified the spectra of the clusters up to large values of N. They found that at $N = 14$ the first coordination sphere of the cluster is filled, since this value corresponds to a sharp decrease in the rate of the vibration frequency shift. When N is small, the cluster spectra have the shape typical of those in nanodroplets, i.e., they consist of three branches corresponding to the symmetric-top model. The rotational constants determined from the molecular spectra decrease rapidly as the cluster size increases, with B being inversely proportional to the number of molecules, and at $N = 11$ it is a hundred times smaller than the rotational constant of a free HCN molecule.

However, the spectrum undergoes a dramatic change at $N = 12$: it consists of one spectral line that is strongly shifted and broadened; the Stark effect enables one to identify it as $R(0)$. The rotational constant B determined from such a spectrum equals 1.4 cm^{-1}, which is greater than its value for pure helium (1.175 cm^{-1} [109]) and is close to the value for the rotation of a free molecule (1.47 cm^{-1} [110]). A similar phenomenon occurs in a cluster with $N = 13$, but here the line is broadened even more and its identification is less reliable. In any case, the chromophore rotates almost freely in the $(HD)_{12}-HCN$ cluster, which means that such rotations may not be related to superfluidity (the reader will recall that the HD molecules are fermions). Hence, a sharp increase in the rotational constant (a decrease in the inertia tensor) near the filling of the first coordination sphere is observed in clusters consisting not only of bosons but also of fermions. In the latter case, however, it is highly improbable that superfluidity can start at 0.3 K.

Thus, the spectroscopy of small clusters of helium and hydrogen have made it possible to study a number of interesting effects, but the question of whether superfluidity manifests itself in objects for which the number of atoms (molecules) is smaller than 50 remains open. Since this area of research is very young (it is not even five years old), we can expect new impressive discoveries.

7. Conclusion

Hence, our consideration reveals that in weakly bound binary van der Waals complexes there are indeed near free rotations of one (He – CO, $para H_2$ – CO, and He – HCN) or both ($para N_2$ – CO and CO – CO) monomers. Here, the total angular momentum is combined from these rotations and the rotations of the complex as a single entity. The process of transformation of the spectra from the rotation of the complex as a whole to the nearly free rotation of a monomer is clearly seen in the Rg – CO series as the mass of the rare gas atom Rg is reduced from xenon to helium.

In He_N-X clusters there is partial entrainment of helium atoms in the rotation of the light molecule, the chromophore X, which manifests itself in the decrease in the moment of inertia with increasing cluster size (CO_2, $N > 5$, and CO, $N > 3$), or its saturation (N_2O, $N > 6$). To within experimental accuracy, this motion is dissipationless. Similar rotation has been detected in the $(para H_2)_N-CO$ clusters with $N > 5$. What is more, nearly free rotations of the CO molecule have been detected in He_N-CO and $(para H_2)_N-CO$. For some compositions, the frequency of this rotation is higher than that of a free molecule. It is still unclear whether there is any relation of these effects to superfluidity.

Acknowledgments. We dedicate this review to the wonderful scientist and person F S Rusin, who turned eighty on November 28, 2006. We would like to express our deep gratitude to G Winnewisser, A R W McKellar, V G Koloshnikov, and S Schlemmer for the fruitful discussions, and to V A Panfilov for his help in preparing the review for press. This work was made possible by grants from the Russian

[19] The reader will recall that superfluidity in ^3He sets in at 2.7 mK.

Foundation for Basic Research and DFG (grant Nos 05-02-04008 and 06-02-16035).

References

1. Toennies J P, Vilesov A F *Angew. Chem. Int. Ed.* **43** 2622 (2004)
2. Makarov G N *Usp. Fiz. Nauk* **174** 225 (2004) [*Phys. Usp.* **47** 217 (2004)]
3. Grebenev S, Toennies J P, Vilesov A F *Science* **279** 2083 (1998)
4. Tang J et al. *Science* **297** 2030 (2002)
5. Chan M-C, McKellar A R W *J. Chem. Phys.* **105** 7910 (1996)
6. McKellar A R W *J. Chem. Phys.* **108** 1811 (1998)
7. Miller D R "Free jet sources", in *Atomic and Molecular Beam Methods* Vol. 1 (Ed. G Scoles) (New York: Oxford Univ. Press, 1988)
8. Tang J, McKellar A R W *J. Chem. Phys.* **119** 754 (2003)
9. Surin L et al., in *Proc. of the 19th Colloquium on High-Resolution Molecular Spectroscopy, Salamanca, 2005, 11 – 16 September*, p. 172
10. Brookes M D et al. *Spectrochim. Acta A* **60** 3235 (2004)
11. Balle T J, Flygare W H *Rev. Sci. Instrum.* **52** 33 (1981)
12. Xu Y, Jäger W *J. Chem. Phys.* **106** 7968 (1997)
13. Dumesh B S et al. *Prib. Tekh. Eksp.* (5) 102 (1992) [*Instrum. Exp. Tech.* **35** 827 (1992)]
14. Rusin F S, Bogomolov G D *Pis'ma Zh. Eksp. Teor. Fiz.* **4** 236 (1966) [*JETP Lett.* **4** 160 (1966)]
15. Surin L A et al. *Phys. Rev. Lett.* **86** 2002 (2001)
16. Surin L A et al. *Rev. Sci. Instrum.* **72** 2535 (2001)
17. Shimoda K, in *Laser Spectroscopy of Atoms and Molecules* (Topics in Applied Physics, Vol. 2, Ed. H Walther) (Berlin: Springer-Verlag, 1976) p. 198
18. Markov V N, Xu Y, Jäger W *Rev. Sci. Instrum.* **69** 4061 (1998)
19. Surin L A et al. *J. Mol. Spectrosc.* **222** 93 (2003)
20. Orville-Thomas W J (Ed.) *Internal Rotation in Molecules* (London: Wiley-Interscience, 1974)
21. Townes C H, Schawlow A L *Microwave Spectroscopy* (New York: McGraw-Hill, 1955) [Translated into Russian (Moscow: IL, 1959)]
22. Chuaqui C E, Le Roy R J, McKellar A R W *J. Chem. Phys.* **101** 39 (1994)
23. Havenith M *Infrared Spectroscopy of Molecular Clusters: An Introduction to Intermolecular Forces* (Springer Tracts in Modern Physics, Vol. 176) (Berlin: Springer-Verlag, 2002)
24. Wormer P E S, van der Avoird A *Chem. Rev.* **100** 4109 (2000)
25. Johns J W C, Lu Z, McKellar A R W *J. Mol. Spectrosc.* **159** 210 (1993)
26. Brookes M D, McKellar A R W *Mol. Phys.* **97** 127 (1999)
27. Walker K A et al. *J. Chem. Phys.* **106** 7519 (1997)
28. Walker K A, McKellar A R W *J. Mol. Spectrosc.* **205** 331 (2001)
29. McKellar A R W *J. Mol. Spectrosc.* **158** 100 (1993)
30. Coudert L H, Pak I, Surin L *J. Chem. Phys.* **121** 4691 (2004)
31. Randall R W et al. *Mol. Phys.* **79** 1113 (1993)
32. McKellar A R W, Chan M-C *Mol. Phys.* **93** 253 (1998)
33. Walker K A et al. *J. Chem. Phys.* **106** 7519 (1997)
34. Winnewisser G et al. *J. Mol. Spectrosc.* **192** 243 (1998)
35. Roth D A et al. *Z. Naturforsch. A* **55** 754 (2000)
36. Surin L A et al. *J. Mol. Spectrosc.* **230** 149 (2005)
37. Moszynski R et al. *J. Phys. Chem. A* **101** 4690 (1997)
38. McBane G C, Cybulski S M *J. Chem. Phys.* **110** 11734 (1999)
39. Subramanian V et al. *Chem. Phys. Lett.* **307** 493 (1999)
40. McKellar A R W et al. *J. Chem. Phys.* **110** 10766 (1999)
41. Surin L A et al. *J. Chem. Phys.* **112** 4064, 9190 (2000)
42. Peterson K A, McBane G C *J. Chem. Phys.* **123** 084314 (2005)
43. Kawashima Y, Nishiza K *Chem. Phys. Lett.* **249** 87 (1996)
44. Xu Y, McKellar A R W *J. Chem. Phys.* **104** 2488 (1996)
45. Xia C, McKellar A R W, Xu Y *J. Chem. Phys.* **113** 525 (2000)
46. Kawashima Y, Ohshima Y, Endo Y *Chem. Phys. Lett.* **315** 201 (1999)
47. Xu Y, Jäger W *J. Chem. Phys.* **113** 514 (2000)
48. Xu Y et al. *J. Chem. Phys.* **111** 10476 (1999)
49. Surin L A et al. *J. Mol. Struct.* **612** 207 (2002)
50. Fišer J, Polák R *Chem. Phys. Lett.* **360** 565 (2002)
51. McKellar A R W *Chem. Phys. Lett.* **186** 58 (1991)
52. McKellar A R W *J. Chem. Phys.* **112** 9282 (2000)
53. Pak I et al. *Chem. Phys. Lett.* **304** 145 (1999)
54. Surin L A et al. *J. Chem. Phys.* **113** 9351 (2000)
55. Jankowski P, Szalewicz K *J. Chem. Phys.* **108** 3554 (1998)
56. Jankowski P, Szalewicz K *J. Chem. Phys.* **123** 104301 (2005)
57. Havenith M, Schwaab G W *Z. Phys. Chem.* **219** 1053 (2005)
58. Surin L A et al. *J. Mol. Struct.* **795** 198 (2006)
59. Tang J, McKellar A R W *J. Chem. Phys.* **119** 754 (2003)
60. Harada K et al. *J. Chem. Phys.* **117** 7041 (2002)
61. Van den Bout P A et al. *Astrophys. J.* **234** 503 (1979)
62. Havenith M et al. *J. Mol. Spectrosc.* **167** 248 (1994)
63. Roth D A et al. *Chem. Phys. Lett.* **298** 381 (1998)
64. Bunker P R et al. *J. Mol. Spectrosc.* **157** 208 (1993)
65. Brookes M D, McKellar A R W *Chem. Phys. Lett.* **287** 365 (1998)
66. Surin L A et al. *J. Chem. Phys.* **112** 4064 (2000)
67. Tang J et al. *J. Mol. Spectrosc.* **214** 87 (2002)
68. Dumesh B S et al. *Pis'ma Zh. Eksp. Teor. Fiz.* **80** 107 (2004) [*JETP Lett.* **80** 98 (2004)]
69. Xu Y, McKellar A R W *Mol. Phys.* **88** 859 (1996)
70. Vissers G W M et al. *J. Chem. Phys.* **122** 054306 (2005)
71. Surin L A et al. *J. Mol. Spectrosc.* **223** 132 (2004)
72. Xu Y, Jäger W *J. Chem. Phys.* **119** 5457 (2003)
73. Tang J, McKellar A R W *J. Chem. Phys.* **119** 5467 (2003)
74. Tang J et al. *Phys. Rev. Lett.* **92** 145503 (2004)
75. Tang J, McKellar A R W *J. Chem. Phys.* **121** 181 (2004)
76. Xu Y et al. *Phys. Rev. Lett.* **91** 163401 (2003)
77. McKellar A R W *J. Chem. Phys.* **121** 6868 (2004)
78. Topik W C, Jäger W, in *Proc. of the 19th Colloquium on High-Resolution Molecular Spectroscopy, Salamanca, 2005, 11 – 16 September*, p. 175
79. Moroni S et al. *Phys. Rev. Lett.* **90** 143401 (2003)
80. Paesani F, Whaley K B *J. Chem. Phys.* **121** 5293 (2004)
81. Paesani F, Kwon Y, Whaley K B *J. Chem. Phys.* **121** 4180 (2004)
82. Moroni S, Blinov N, Roy P-N *J. Chem. Phys.* **121** 3577 (2004)
83. Nauta K, Miller R E *J. Chem. Phys.* **115** 10254 (2001)
84. McKellar A R W, in *Proc. of the 19th Colloquium on High-Resolution Molecular Spectroscopy, Salamanca, 2005, 11 – 16 September*, p. 173
85. Cazzato P et al. *J. Chem. Phys.* **120** 9071 (2004)
86. von Haeften K et al. *Phys. Rev. B* **73** 054502 (2006)
87. Xu Y, Jäger W, in *Book of Abstracts of 59th Intern. Symp. on Molecular Spectroscopy, Columbus, June 21 – 25, 2004*, p. 144
88. Zillich R E et al. *J. Chem. Phys.* **123** 114301 (2005)
89. Ginzburg V L, Sobyanin A A *Pis'ma Zh. Eksp. Teor. Fiz.* **15** 343 (1972) [*JETP Lett.* **15** 242 (1972)]
90. Apenko S M *Phys. Rev. B* **60** 3052 (1999)
91. Vorob'ev V S, Malyshenko S P *J. Phys.: Condens. Matter* **12** 5071 (2000)
92. Sindzingre P, Ceperley D M, Klein M L *Phys. Rev. Lett.* **67** 1871 (1991)
93. Grebenev S et al. *Science* **289** 1532 (2000)
94. Moroni S et al. *J. Chem. Phys.* **122** 094314 (2005)
95. Tang J, McKellar A R W *J. Chem. Phys.* **123** 114314 (2005)
96. Tang J, McKellar A R W *J. Chem. Phys.* **121** 3087 (2004)
97. Tang J, McKellar A R W *J. Chem. Phys.* **117** 8308 (2002)
98. Paesani F, Zillich R E, Whaley K B *J. Chem. Phys.* **119** 11682 (2003)
99. Grebenev S et al. *J. Chem. Phys.* **118** 8656 (2003)
100. Grebenev S et al. *Phys. Rev. Lett.* **89** 225301 (2002)
101. El'tsov V B, Parshin A Ya, Todoshchenko I A *Zh. Eksp. Teor. Fiz.* **108** 1657 (1995) [*JETP* **81** 909 (1995)]
102. Babichenko V S, Kagan Yu *Phys. Rev. Lett.* **83** 3458 (1999); Lehmann K K *Mol. Phys.* **97** 645 (1999)
103. Callegari C et al. *J. Chem. Phys.* **113** 4636 (2000)
104. Callegari C et al. *J. Chem. Phys.* **115** 10090 (2001)
105. Andronikashvili E L *Zh. Eksp. Teor. Fiz.* **16** 780 (1946); **18** 424 (1948); *J. Phys. USSR* **10** 201 (1946)
106. Paesani F, Kwon Y, Whaley K B *Phys. Rev. Lett.* **94** 153401 (2005)
107. Paesani F et al. *J. Chem. Phys.* **122** 181106 (2005)
108. Moore D T, Miller R E *J. Chem. Phys.* **119** 4713 (2003)
109. Nauta K, Miller R E *Phys. Rev. Lett.* **82** 4480 (1999)
110. Smith A M et al. *J. Mol. Spectrosc.* **134** 134 (1989)
111. Xu Y et al. *J. Chem. Phys.* **124** 081101 (2006)